

# Continuous Multiclass Labeling Approaches and Algorithms

J. Lellmann<sup>†</sup>      C. Schnörr<sup>†</sup>

January 13, 2013

## Abstract

We study convex relaxations of the image labeling problem on a continuous domain with regularizers based on metric interaction potentials. The generic framework ensures existence of minimizers and covers a wide range of relaxations of the originally combinatorial problem. We focus on two specific relaxations that differ in flexibility and simplicity – one can be used to tightly relax any metric interaction potential, while the other one only covers Euclidean metrics but requires less computational effort. For solving the nonsmooth discretized problem, we propose a globally convergent Douglas-Rachford scheme, and show that a sequence of dual iterates can be recovered in order to provide a posteriori optimality bounds. In a quantitative comparison to two other first-order methods, the approach shows competitive performance on synthetic and real-world images. By combining the method with an improved binarization technique for non-standard potentials, we were able to routinely recover discrete solutions within 1%–5% of the global optimum for the combinatorial image labeling problem.

## 1 Problem Formulation

The multi-class image labeling problem consists in finding, for each pixel  $x$  in the image domain  $\Omega \subseteq \mathbb{R}^d$ , a label  $\ell(x) \in \{1, \dots, l\}$  which assigns one of  $l$  class labels to  $x$  so that the labeling function  $\ell$  adheres to some local data fidelity as well as nonlocal spatial coherency constraints.

This problem class occurs in many applications, such as segmentation, multiview reconstruction, stitching, and inpainting [PCF06]. We consider the variational formulation

$$\inf_{\ell: \Omega \rightarrow \{1, \dots, l\}} f(\ell), \quad f(\ell) := \underbrace{\int_{\Omega} s(x, \ell(x)) dx}_{\text{data term}} + \underbrace{J(\ell)}_{\text{regularizer}}. \quad (1)$$

The *data term* assigns to each possible label  $\ell(x)$  a *local cost*  $s(x, \ell(x)) \in \mathbb{R}$ , while the *regularizer*  $J$  enforces the desired spatial coherency. We will in particular be interested in regularizers that penalize the weighted length of interfaces

---

<sup>†</sup>Image and Pattern Analysis & HCI, Dept. of Mathematics and Computer Science, University of Heidelberg, {lellmann,schnoerr}@math.uni-heidelberg.de

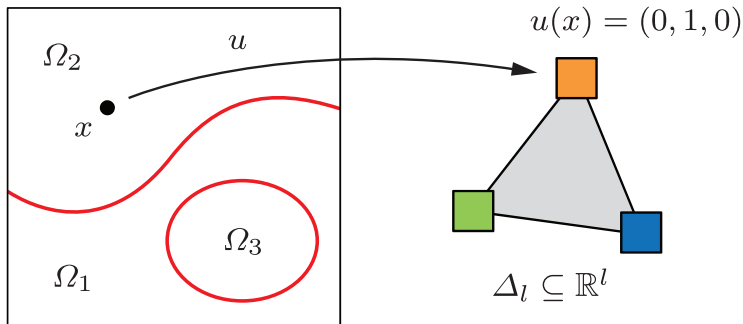


Figure 1: Convex relaxation of the multiclass labeling problem. The assignment of one unique label to each point in the image domain  $\Omega$  is represented by a vector-valued function  $u : \Omega \rightarrow \mathbb{R}^l$ . Ideally,  $u$  partitions the image into  $l$  sets by assuming one of the unit vectors  $\{e^1, \dots, e^l\}$  everywhere. By relaxing this set to the standard (probability) simplex  $\Delta_l$ , the originally combinatorial problem can be treated in a convex framework.

between regions of constant labeling. Minimizing  $f$  is an inherently combinatorial problem, as there is a discrete decision to be made for each point in the image.

In the fully discrete setting, the problem can be expressed in terms of a Markov Random Field [Win06] with a discrete state space, where the data and regularization terms can be thought of as unary and binary potentials, respectively. For graph-based discretizations of  $J$ , the resulting objective only contains terms that depend on the labels at one or two points, and the problem can be approached with fast graph cut-based methods. Unfortunately, this scheme introduces an anisotropy [Boy03] and thus does not represent isotropic regularizers well. Using ternary or higher-order terms, the metrication error can be reduced, but graph-based methods then cannot be directly applied.

However, it can be shown that even in the graph-based representation the problem is NP-hard for relatively simple  $J$  [BVZ01], so we cannot expect to easily derive fast solvers for this problem. This is in part caused by the discrete nature of the feasible set. In the following, we will relax this set. This allows to solve the problem in a globally optimal way using convex optimization methods. On the downside, we cannot expect the relaxation to be exact for any problem instance, i.e. we might get non-discrete (or discrete but suboptimal) solutions.

There are several choices for the relaxation method, of which in our opinion the following is the most transparent (Fig. 1): Identify label  $i$  with the  $i$ -th unit vector  $e^i \in \mathbb{R}^l$ , set  $E := \{e^1, \dots, e^l\}$ , and solve

$$\inf_{u: \Omega \rightarrow E} f(u), \quad f(u) := \int_{\Omega} \langle u(x), s(x) \rangle dx + J(u). \quad (2)$$

The data term is now linear in  $u$  and fully described by the vector

$$s(x) := (s_1(x), \dots, s_l(x))^{\top} := (s(x, 1), \dots, s(x, l))^{\top}. \quad (3)$$

Due to the linearization, the local costs  $s$  may be arbitrarily complicated, possibly derived from a probabilistic model, without affecting the overall problem

class. In this form, we *relax* the label set by allowing  $u$  to take “intermediate” values in the convex hull  $\text{conv } E$  of the original label set. This is just the standard simplex  $\Delta_l$ ,

$$\Delta_l := \text{conv}\{e^1, \dots, e^l\} = \{a \in \mathbb{R}^l \mid a \geq 0, \sum_{i=1}^l a_i = 1\}. \quad (4)$$

The problem is then considered on the relaxed feasible set  $\mathcal{C}$ ,

$$\mathcal{C} := \{u \in \text{BV}(\Omega)^l \mid u(x) \in \Delta_l \text{ for a.e. } x \in \Omega\}. \quad (5)$$

The space of functions of bounded variation  $\text{BV}(\Omega)^l \subset (L^1)^l$  guarantees a minimal regularity of the discontinuities of  $u$ , see Sect. 2.2. Assuming we can extend the regularizer  $J$  to the whole relaxed set  $\mathcal{C}$ , we get the relaxed problem

$$\inf_{u \in \mathcal{C}} f(u), \quad f(u) := \int_{\Omega} \langle u(x), s(x) \rangle dx + J(u). \quad (6)$$

If  $J$  can be made convex, the overall problem is convex as well, and it may likely be computationally tractable. In addition,  $J$  should ideally have a closed-form expression, or at least lead to a computationally tractable problem.

Whether these points are satisfied depends on the way a given regularizer is *extended* to the relaxed set. The prototypical example for such a regularizer is the *total variation*,

$$\text{TV}(u) = \int_{\Omega} \|Du\|, \quad (7)$$

where  $\|\cdot\|$  denotes the Frobenius norm, in this case on  $\mathbb{R}^{d \times l}$ . Note that  $u$  may be discontinuous, so the gradient  $Du$  has to be understood in a distributional sense (Sect. 2.2). Much of the popularity of TV stems from the fact that it allows to include *boundary-length* terms: The total variation of the indicator function  $\chi_S$  of a set  $S$ ,

$$\text{Per}(S) := \text{TV}(\chi_S). \quad (8)$$

called the *perimeter* of  $S$ , is just the classical length of the boundary  $\partial S$ .

In this paper, we will in more generality consider ways to construct regularizers which penalize interfaces between two adjacent regions with labels  $i \neq j$  according to the *perimeter* (i.e. length or area) of the interface weighted by an *interaction potential*  $d : \{1, \dots, l\}^2 \rightarrow \mathbb{R}$  depending on the labels (in a slight abuse of notation the interaction potential is also denoted by  $d$ , since there is rarely any ambiguity with respect to the ambient space dimension). The simplest case is the *Potts* model with the *uniform* metric  $d(i, j) = 0$  iff  $i = j$  and otherwise  $d(i, j) = 1$ . In this case, the regularizer penalizes the total interface length, as seen above for the total variation.

As a prime motivation for our work, consider the two-class case  $l = 2$  with  $J = \text{TV}$ . As here the second component of  $u$  is given by the first via  $u_2 = 1 - u_1$ , we may pose the relaxed problem in the form

$$\min_{\substack{u' \in \text{BV}(\Omega), \\ u'(x) \in [0,1] \text{ for a.e. } x \in \Omega}} \int_{\Omega} u'(x)(s_1(x) - s_2(x))dx + 2 \text{TV}(u'), \quad (9)$$

where  $u'(x)$  is a scalar. This formulation is also referred to as *continuous cut* in analogy to graph cut methods. It can be shown [CEN06] that while there may be non-discrete solutions of the relaxed problem, a *discrete* – i.e.  $u'(x) \in \{0, 1\}$  – global optimal solution can be recovered from *any* solution of the relaxed problem. We can thus reduce the *combinatorial* problem to a *convex* problem. While there are reasons to believe that this procedure cannot be extended to the multi-class case, we may still hope for “nearly” discrete solutions.

## 1.1 Related Work

The difficulty of the labeling problem varies greatly with its precise definition. Formulations of the labeling problem can be categorized based on

1. whether they tackle the binary (two-class) or the much harder multiclass problem, and
2. whether they rely on a graph representation or are formulated in a spatially continuous framework.

An early analysis of a variant of the *binary continuous* cut problem and the associated dual *maximal flow* problem was done by Strang [Str83]. Chan et al. [CEN06] pointed out that by thresholding a nonbinary result of the relaxed, convex problem at almost any threshold one can generate binary solutions of the original, combinatorial problem (this can be carried over to *any* threshold and to slightly more general regularizers [Ber09, ZNF09]. The proof heavily relies on the coarea formula [FR60], which unfortunately does not transfer to the multiclass case. The binary continuous case is also closely related to the thoroughly analyzed Mumford-Shah [MS89] and Rudin-Osher-Fatemi (ROF) [ROF92] problems, where a quadratic data term is used.

For the *graph-based* discretization, the binary case can be formulated as a minimum-cut problem on a grid graph, which allows to solve the problem exactly and efficiently for a large class of metrics using graph cuts [KB05, BK04]. Graph cut algorithms have become a working horse in many applications as they are very fast for medium sized problems. Unfortunately they offer hardly any potential for parallelization. As mentioned in the introduction, the graph representation invariably introduces a grid bias [Boy03] (Fig. 2). While it is possible to reduce the resulting artifacts by using larger neighborhoods, or by moving higher-order potentials through factor graphs, this greatly increases graph size as well as processing time.

Prominent methods to handle the graph-based *multiclass* case rely on finding a local minimum by solving a sequence of binary graph cuts [BVZ01] (see [KT07] for a recent generalization). These methods have recently been extended to the continuous formulation [TPCB08] with similar theoretical performance [Ols09]. Our results can be seen as a continuous analogon to [Ish03], where it was shown that potentials of the form  $d(i, j) = |i - j|$  can be exactly formulated as a cut on a multi-layered graph. An early analysis can be found in [KT99], where the authors also derive suboptimality bounds of a linear programming relaxation for metric distances. All these methods rely on the graph representation with pairwise potentials.

In this paper, we will focus on the *continuous multiclass* setting with higher order potentials in the discretization. Closely related to our approach is [CCP08].

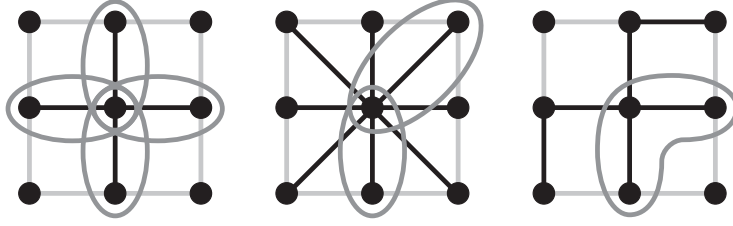


Figure 2: Discretization schemes. **Left to right:** Graph-based with 4- and 8-neighborhood; higher order potentials. In graph-based approaches the regularizer is discretized using terms depending on the labels of at most two neighboring points. This leads to artifacts as isotropic metrics are not approximated well. Using higher-order terms the discrete functional more closely approximates the continuous functional (Fig. 3).



Figure 3: Effect of the discretization on an inpainting problem. **Left to right:** Input image with unknown black region; graph-based method using pairwise potentials ( $\alpha$ - $\beta$ -swap code from [SZS<sup>+</sup>06]); proposed method using higher order potentials. Due to the introduced anisotropy, the graph-based method shows a bias towards axis-parallel edges.

In contrast to approaches that rely on a linear ordering of the labels [Ish03, BT09], the authors represent labels in a higher-dimensional space. In a certain sense, [LLT06] can be seen as a predecessor of this approach: in this work, the authors represent the label assignment using a piecewise constant real-valued function, but parametrize this function using a set of  $l$  polynomial basis functions, which enables them to employ the Potts regularizer.

The approach of [CCP08] allows to formulate interaction potentials of the form  $d(i, j) = \gamma(|i - j|)$  with nondecreasing, positive, concave  $\gamma$ . The authors provide a thorough analysis of the continuous model and propose a relaxation based on the convex envelope, which gives almost discrete solutions in many cases. We will extend this approach to the more general class of regularizers where  $d$  is an arbitrary metric. The same authors proposed a “Fast Primal-Dual” algorithm with proven convergence to solve the associated saddle point problem [PCBC09a]. By lifting the objective to a higher dimensional space, it turns out that the same method can be used to solve many problems also with nonlinear data term [PCBC09b].

Our approach is a generalization of [ZGFN08, LKY<sup>+</sup>09], where a similar linearization is used with the regularizer restricted to the Potts distance, and with less strong convergence results. These methods have also been extended

to segmentation on manifolds [DFPH09].

Regarding optimization, several authors proposed smoothing of the primal or dual objective together with gradient descent [Ber09, BYT10]. In contrast, our approach does not require any a priori smoothing. Using Nesterov’s method [Nes04] for the labeling problem was proposed in [LKY<sup>+</sup>09]. An earlier analysis of the method in the context of  $\ell_1$ -norm and TV minimization can be found in [WABF07]. In [BBC09] the method is applied to a class of general  $\ell_1$  regularized problems. In [GBO09] a predecessor of the proposed Douglas-Rachford approach was presented in the Split Bregman framework [Set09a] and restricted to the two-class case. We provide an extension to the multi-class case, with proof of convergence and a sound stopping criterion.

## 1.2 Contribution

The paper is organized as follows:

1. We formulate natural requirements on the regularizer  $J$  and show their implications on the choice of the interaction potential  $d$  (Sect. 3). In particular,  $d$  must necessarily be a metric under these requirements (Prop. 1).
  2. Given such a metric, we study two possible approaches to extend regularizers  $J$  on the relaxed set (Sect. 4):
    - The “envelope” approach, which is a generalization of the method recently suggested by Chambolle et al. (Sect. 4.3). While there is no simple closed form expression, we show that it can be used to construct a true extension for *any* metric  $d$  (Prop. 5).
    - The “Euclidean distance” approach (Sect. 4.4), which yields exact extensions for Euclidean metrics  $d$  only but has a closed form expression. We review some methods for the approximation of non-Euclidean metrics.
- We provide a unified continuous framework and show existence of a minimizer.
3. Both approaches lead to non-smooth convex problems, which can be studied in a general saddle point formulation (Sect. 5). Within this framework, we propose an improved binarization technique for nonstandard potentials to recover approximate solutions for the non-relaxed problem (Sect. 5.6).
  4. We provide and analyze two different methods that are capable of minimizing the specific class of saddle point problems (Sect. 6):
    - A specialization of a method for nonsmooth optimization as suggested by Nesterov (Sect. 6.2). The method is virtually parameter-free and provides explicit a priori and a posteriori optimality bounds.
    - A Douglas-Rachford splitting approach (Sect. 6.3). We show that the approach allows to compute a sequence of dual iterates that provide an optimality bound and stopping criterion in form of the primal-dual gap.

Both methods are highly parallelizable and are shown to converge. For reference, we also summarize the primal-dual technique from [PCBC09a] (Sect. 6.1).

5. Finally, we illustrate and compare the above methods under varying conditions and demonstrate the applicability of the proposed approaches on real-world problems (Sect. 7).

In contrast to existing graph-based methods, we provide a continuous and isotropic formulation, while in comparison with existing continuous approaches, we provide a unified framework for arbitrary, non-uniform metrics  $d$ . The Euclidean metric method and Nesterov optimization have been announced in less generality in [LKY<sup>+</sup>09, LBS09].

## 2 Mathematical Preliminaries

In the following sections we provide a reference of the notation used, and a brief introduction to the concept of functions of bounded variation and corresponding functionals. We aim to provide the reader with the basic ideas. For more detailed expositions we refer to [AFP00, Zie89].

### 2.1 Notation

In the following, superscripts  $v^i$  denote a collection of vectors or matrix columns, while subscripts  $v_k$  denote vector components, i.e. we denote, for  $A \in \mathbb{R}^{d \times l}$ ,

$$A = (a^1 | \dots | a^l) = (A_{ij}), \quad A_{ij} = (a^j)_i = a_i^j, \quad 1 \leq i \leq d, 1 \leq j \leq l. \quad (10)$$

An additional bracket  $v^{(i)}$  indicates an element of a sequence  $(v^{(i)})$ . We will frequently make use of the Kronecker product [Gra81]

$$\otimes : \mathbb{R}^{n_1 \times m_1} \times \mathbb{R}^{n_2 \times m_2} \rightarrow \mathbb{R}^{(n_1 n_2) \times (m_1 m_2)} \quad (11)$$

in order to formulate all results for arbitrary dimensions. The standard simplex in  $\mathbb{R}^l$  is denoted by  $\Delta_l := \{x \in \mathbb{R}^l | x \geq 0, e^\top x = 1\}$ , where  $e := (1, \dots, 1)^\top \in \mathbb{R}^l$ .  $I_n$  is the identity matrix in  $\mathbb{R}^n$  and  $\|\cdot\|$  the usual Euclidean norm for vectors resp. the Frobenius norm for matrices. Analogously, the standard inner product  $\langle \cdot, \cdot \rangle$  extends to pairs of matrices as the sum over their elementwise product.  $\mathcal{B}_r(x)$  denotes the ball of radius  $r$  at  $x$ , and  $S^{d-1}$  the set of  $x \in \mathbb{R}^d$  with  $\|x\| = 1$ . The characteristic function  $\chi_S(x)$  of a set  $S$  is defined as  $\chi_S(x) = 1$  iff  $x \in S$  and  $\chi_S(x) = 0$  otherwise. By  $\delta_S(x) = 0$  iff  $x \in S$  and  $\delta_S(x) = +\infty$  otherwise we denote the corresponding indicator function. For a convex set  $\mathcal{C}$ ,  $\sigma_{\mathcal{C}}(u) := \sup_{v \in \mathcal{C}} \langle u, v \rangle$  is the support function from convex analysis.  $\mathcal{J}(u)$  denotes the classical Jacobian of  $u$ .

$C_c^k(\Omega)$  is the space of  $k$ -times continuously differentiable functions on  $\Omega$  with compact support, and  $C_0(\Omega)$  the completion of  $C_c^0(\Omega)$  under the supremum norm. As usual,  $\mathcal{L}^d$  denotes the  $d$ -dimensional Lebesgue measure, while  $\mathcal{H}^k$  denotes the  $k$ -dimensional Hausdorff measure. For some measure  $\mu$  and set  $M$ ,  $\mu \llcorner M$  denotes the restriction of  $\mu$  to  $M$ , i.e.  $(\mu \llcorner M)(A) := \mu(M \cap A)$ .

## 2.2 Total Variation and BV

The total variation will be our main tool to construct the regularizer  $J$ . For a differentiable scalar-valued function  $u$ , the total variation is simply the integral over the norm of its gradient:

$$\text{TV}(u) = \int_{\Omega} \|\nabla u\| dx. \quad (12)$$

As  $u$  is the designated labeling function, which ideally should be piecewise constant, the differentiability and continuity assumptions have to be dropped. In the following we will shortly review the general definition of the total variation and its properties.

We require the image domain  $\Omega \subseteq \mathbb{R}^d$  to be a bounded open domain with compact Lipschitz boundary, that is the boundary can locally be represented as the graph of a Lipschitz-continuous function. For simplicity, we will assume in the following that  $\Omega = (0, 1)^d$ .

We consider general vector-valued functions  $u = (u_1, \dots, u_l) : \Omega \rightarrow \mathbb{R}^l$  which are locally absolutely integrable, i.e.  $u \in L^1_{\text{loc}}(\Omega)^l$ . As  $\Omega$  is bounded this is equivalent to being absolutely integrable, i.e.  $u \in L^1(\Omega)^l$ . For any such function  $u$ , its *total variation*  $\text{TV}(u)$  is defined in a dual way [AFP00, (3.4)] as

$$\text{TV}(u) := \sup_{v \in \mathcal{D}^{\text{TV}}} \sum_{j=1}^l \int_{\Omega} u_j \operatorname{div} v^j dx = \sup_{v \in \mathcal{D}^{\text{TV}}} \int_{\Omega} \langle u, \operatorname{Div} v \rangle dx, \quad (13)$$

$$\mathcal{D}^{\text{TV}} := \{v \in C_c^\infty(\Omega)^{d \times l} \mid \|v(x)\| \leq 1 \ \forall x \in \Omega\}, \quad (14)$$

$$\operatorname{Div} v := (\operatorname{div} v^1, \dots, \operatorname{div} v^l)^\top.$$

This definition can be derived for continuously differentiable  $u$  by extending (12) to vector-valued  $u$ ,

$$\text{TV}(u) = \int_{\Omega} \|\mathcal{J}(u)\| dx, \quad (15)$$

replacing the norm by its dual formulation and partial integration. If  $u$  has finite total variation, i.e.  $\text{TV}(u) < \infty$ ,  $u$  is said to be of *bounded variation*. The vector space of all such functions is denoted by  $\text{BV}(\Omega)^l$ :

$$\text{BV}(\Omega)^l = \left\{ u \in (L^1(\Omega))^l \mid \text{TV}(u) < \infty \right\}. \quad (16)$$

Equivalently,  $u \in \text{BV}(\Omega)^l$  iff  $u \in L^1(\Omega)^l$  and its distributional derivative corresponds to a finite Radon measure; i.e.  $u_j \in L^1(\Omega)$  and there exist  $\mathbb{R}^d$ -valued measures  $Du_j = (D_1 u_j, \dots, D_d u_j)$  on the Borel subsets  $\mathcal{B}(\Omega)$  of  $\Omega$  such that [AFP00, p.118]

$$\sum_{j=1}^l \int_{\Omega} u_j \operatorname{div} v^j dx = - \sum_{j=1}^l \sum_{i=1}^d \int_{\Omega} v_i^j dD_i u_j, \quad \forall v \in (C_c^\infty(\Omega))^{d \times l}. \quad (17)$$

These measures form the distributional gradient  $Du = (Du_1 | \dots | Du_l)$ , which is again a measure that vanishes on any  $\mathcal{H}^{(d-1)}$ -negligible set. If  $u \in \text{BV}(\Omega)$  then  $|Du|(\Omega) = \text{TV}(u)$ , where  $|Du|$  is the total variation of the measure  $Du$  in the measure-theoretic sense [AFP00, 3.6]. The total variation of characteristic functions has an intuitive geometrical interpretation: For a Lebesgue-measurable



subset  $\mathcal{S} \subseteq \mathbb{R}^d$ , its *perimeter* is defined as the total variation of its characteristic function,

$$\text{Per}(\mathcal{S}) := \text{TV}(\chi_{\mathcal{S}}). \quad (18)$$

Assuming the boundary  $\partial\mathcal{S}$  is sufficiently regular,  $\text{Per}(\mathcal{S})$  is just the classical length ( $d = 2$ ) or area ( $d = 3$ ) of the boundary.

### 2.3 Properties of TV and Compactness

We review the most important ingredients for proving existence of minimizers for variational problems on involving BV involving TV.

*Convexity.* As TV is the pointwise supremum of a family of linear functions, it is *convex* and *positively homogeneous*, i.e.  $\text{TV}(\alpha u) = \alpha \text{TV}(u)$  for  $\alpha > 0$ .

*Lower Semicontinuity.* A functional  $J$  is said to be *lower semicontinuous* with respect to some topology, if for any sequence  $(u^{(k)})$  converging to  $u$ ,

$$\liminf_{k \rightarrow \infty} J(u^{(k)}) \geq J(u). \quad (19)$$

It can be shown that for fixed  $\Omega$ , the total variation TV is well-defined on  $L^1_{\text{loc}}(\Omega)^l$  and lower semicontinuous in  $\text{BV}(\Omega)^l$  w.r.t. the  $L^1_{\text{loc}}(\Omega)^l$  topology [AFP00, 3.5, 3.6]; hence also in  $L^1(\Omega)^l$  due to the boundedness of  $\Omega$ .

*Compactness.* For BV, instead of the norm topology induced by

$$\|u\|_{\text{BV}} := \int_{\Omega} \|u\| dx + \text{TV}(u), \quad (20)$$

which makes  $\text{BV}(\Omega)^l$  a Banach space but is often too strong, one frequently uses the weak\* convergence: Define  $u^{(k)} \rightarrow u$  *weakly\** iff

1.  $u, u^{(k)} \in \text{BV}(\Omega)^l \forall k \in \mathbb{N}$ ,
2.  $u^{(k)} \rightarrow u$  in  $L^1(\Omega)$  and
3.  $Du^{(k)} \rightarrow Du$  weakly\* in measure, i.e.

$$\forall v \in C_0(\Omega) : \lim_{k \rightarrow \infty} \int_{\Omega} v dDu^{(k)} = \int_{\Omega} v dDu. \quad (21)$$

For  $u, u^{(k)} \in \text{BV}(\Omega)^l$  this is equivalent to  $u^{(k)} \rightarrow u$  in  $L^1(\Omega)^l$ , and  $(u^{(k)})$  being uniformly bounded in  $\text{BV}(\Omega)^l$ , i.e. there exists a constant  $C < \infty$  such that  $\|u^{(k)}\|_{\text{BV}} \leq C \forall k \in \mathbb{N}$  [AFP00, 3.13]. For the weak\* topology in BV, a compactness result holds [AFP00, 3.23]: If  $(u^{(k)}) \subset \text{BV}(\Omega)^l$  and  $(u^{(k)})$  is uniformly bounded in  $\text{BV}(\Omega)^l$ , then  $(u^{(k)})$  contains a subsequence weakly\*-converging to some  $u \in \text{BV}(\Omega)^l$ .

### 2.4 General Functionals on BV

We will now review how general functionals depending on the distributional gradient  $Du$  can be defined. Recall that for any  $u \in \text{BV}(\Omega)^l$  the distributional gradient  $Du$  is a measure. Moreover, it can be uniquely decomposed into three mutually singular measures

$$Du = D^a u + D^j u + D^c u, \quad (22)$$

that is: An *absolutely continuous* part  $D^a$ , the *jump* part  $D^j$ , and the *Cantor* part  $D^c$ . Mutual singularity refers to the fact that  $\Omega$  can be partitioned into three subsets, such that each of the measures is concentrated on exactly one of the sets. We will give a short intuitive explanation, see [AFP00, 3.91] for the full definitions.

The  $D^a$  part is absolutely continuous with respect to the  $d$ -dimensional Lebesgue measure  $\mathcal{L}^d$ , i.e. it vanishes on any  $\mathcal{L}^d$ -negligible set. It captures the “smooth” variations of  $u$ : in any neighborhood where  $u$  has a (possibly weak) Jacobian  $\mathcal{J}(u)$ , the jump and Cantor parts vanish and

$$Du = D^a u = \mathcal{J}(u) \mathcal{L}^d. \quad (23)$$

The jump part  $D^j$  is concentrated on the set of points where locally  $u$  jumps between two values  $u^-$  and  $u^+$  along a  $(d-1)$ -dimensional hypersurface with normal  $\nu_u \in S^{d-1}$  (unique up to a change of sign). In fact, there exists a *jump set*  $J_u$  of discontinuities of  $u$  and Borel functions  $u^+, u^- : J_u \rightarrow \mathbb{R}^l$  and  $\nu_u : J_u \rightarrow S^{d-1}$  such that [AFP00, 3.78, 3.90]

$$D^j u = Du \llcorner J_u = \nu_u (u^+ - u^-)^\top \mathcal{H}^{d-1} \llcorner J_u, \quad (24)$$

where  $\mathcal{H}^{d-1} \llcorner J_u$  denotes the restriction of the  $(d-1)$ -dimensional Hausdorff measure on the jump set  $J_u$ , i.e.  $(\mathcal{H}^{d-1} \llcorner J_u)(A) = \mathcal{H}^{d-1}(J_u \cap A)$  for measurable sets  $A$ . The Cantor part  $D^c$  captures anything that is left.

As an important consequence of the mutual singularity, the total variation decomposes into  $|Du| = |D^a u| + |D^j u| + |D^c u|$ . Using this idea, one can define functionals depending on the distributional gradient  $Du$  [AFP00, Prop. 2.34]. For  $u \in \text{BV}(\Omega)^l$  and some convex, lower semi-continuous  $\Psi : \mathbb{R}^{d \times l} \rightarrow \mathbb{R}$ , define

$$\begin{aligned} J(u) &:= \int_{\Omega} \Psi(Du) := \int_{\Omega} \Psi(\mathcal{J}(u)(x)) dx + \dots \\ &\quad \int_{J_u} \Psi_{\infty} \left( \nu_u(x) (u^+(x) - u^-(x))^\top \right) d\mathcal{H}^{d-1} + \dots \\ &\quad \int_{\Omega} \Psi_{\infty} \left( \frac{D^c u}{|D^c u|} \right) d|D^c u|. \end{aligned} \quad (25)$$

Here  $\Psi_{\infty}$  is the recession function  $\Psi_{\infty}(x) = \lim_{t \rightarrow \infty} \frac{\Psi(tx)}{t}$  of  $\Psi$ , and  $D^c u / |D^c u|$  denotes the *polar decomposition* of  $D^c u$ , which is the density of  $D^c u$  with respect to its total variation measure  $|D^c u|$ . If  $\Psi$  is positively homogeneous,  $\Psi_{\infty} = \Psi$  holds, and

$$J(u) = \int_{\Omega} \Psi \left( \frac{Du}{|Du|} \right) d|Du|. \quad (26)$$

From (25) it becomes clear that the meaning of  $\Psi$  acting on the *Jacobian* of  $u$  is extended to the jump set as acting on the *difference* of the left and right side limits of  $u$  at the discontinuity. This is a key point: by switching to the measure formulation, one can handle noncontinuous functions as well.

### 3 Necessary Properties of the Interaction Potential

Before applying the methods above to the labeling problem, we start with some basic considerations about the regularizer and the interaction potential  $d$ . We begin by formalizing the requirements on the regularizer of the relaxed problem as mentioned in the introduction. Let us assume we are given a general interaction potential  $d : \{1, \dots, l\}^2 \rightarrow \mathbb{R}$ . Intuitively,  $d(i, j)$  assigns a weight to switching between label  $i$  and label  $j$ . We require

$$d(i, j) > 0, i \neq j, \quad (27)$$

but no other metric properties (i.e. symmetry or triangle inequality) for now. Within this work, we postulate that the regularizer should satisfy

- (P1)  $J$  is convex and positively homogeneous on  $\text{BV}(\Omega)^l$ .
- (P2)  $J(u) = 0$  for any constant  $u$ , i.e. there is no penalty for constant labelings.
- (P3) For any partition of  $\Omega$  into two sets  $S, S^c$  with  $\text{Per}(S) < \infty$ , and any  $i, j \in \{1, \dots, l\}$ ,

$$J(e^i \chi_S + e^j \chi_{S^c}) = d(i, j) \text{Per}(S), \quad (28)$$

i.e. a change from label  $i$  to label  $j$  gets penalized proportional to  $d(i, j)$  as well as the perimeter of the interface. Note that this implies that  $J$  is isotropic (i.e. rotationally invariant).

We require convexity in (P1) in order to render global optimization tractable. Indeed, if  $J$  is convex, the overall objective function (6) will be convex as well due to the linearization of the data term. Positive homogeneity is included as it allows  $J$  to be represented as a support function (i.e. its convex conjugate is an indicator function and  $J = \sigma_{\mathcal{D}}$  for some closed convex set  $\mathcal{D}$ ), which will be exploited by our optimization methods.

Requirements (P3) and (P2) formalize the principle that the multilabeling problem should reduce to the classical continuous cut (9) in the two-class case. This allows to include boundary length-based terms in the regularizer that can additionally be weighted depending on the labels of the adjoining region (Fig. 4). Together, these requirements pose a natural restriction on  $d$ :

**Proposition 1.** *Let  $(J, d)$  satisfy (P1) – (P3). Then  $d$  must necessarily be a metric, i.e. for all  $i, j, k \in \{1, \dots, l\}$ ,*

1.  $d(i, i) = 0$ ,
2.  $d(i, j) = d(j, i), \forall i \neq j$ ,
3.  $d$  is subadditive:  $d(i, k) \leq d(i, j) + d(j, k)$ .

*Proof.* 1. follows from (P2) and (P3) by choosing  $i = j$  and  $S$  with  $\text{Per}(S) > 0$ . Symmetry in 2. is obtained from (P3) by replacing  $S$  with  $S^c$ , as  $\text{Per}(S) = \text{Per}(S^c)$ . To show 3., first note that  $J(u) = 2J(u/2 + c/2)$  for any constant

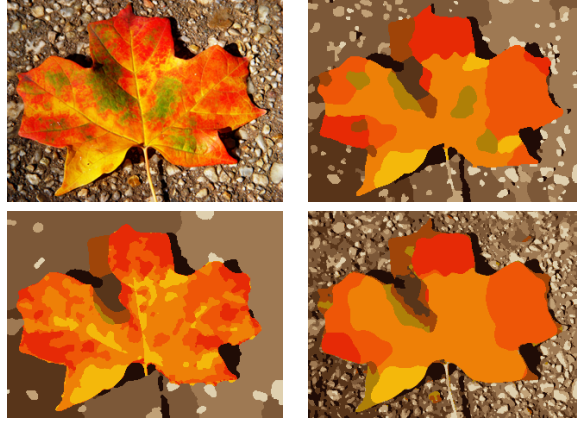


Figure 4: Effect of choosing different interaction potentials. **Top row:** The original image (left) is segmented into 12 regions corresponding to prototypical colors vectors. The Potts interaction potential penalizes the boundary length independently of the labels (right), which leads to a uniformly smooth segmentation. **Bottom row:** By modifying the interaction potential, the regularization strength is selectively adjusted to suppress background (left) or foreground (right) structures while allowing for fine details in the other regions.

$c \in \mathbb{R}^l$  and all  $u \in \text{BV}(\Omega)^l$ , since  $J(u) = J(u+c-c) \leq 2J((u+c)/2) + J(-c/2) = 2J(u/2 + c/2) \leq J(u) + J(c) = J(u)$ . Fix any set  $S$  with perimeter

$$c := \text{Per}(S) > 0. \quad (29)$$

Then, using the above mentioned fact and the positive homogeneity of  $J$ ,

$$cd(i, k) = J(e^i \chi_S + e^k \chi_{S^c}) \quad (30)$$

$$= 2J\left(\frac{1}{2}(e^i \chi_S + e^k \chi_{S^c}) + \frac{1}{2}e^j\right) \quad (31)$$

$$= 2J\left(\frac{1}{2}(e^i \chi_S + e^j \chi_{S^c}) + \frac{1}{2}(e^j \chi_S + e^k \chi_{S^c})\right) \quad (32)$$

$$\leq J(e^i \chi_S + e^j \chi_{S^c}) + J(e^j \chi_S + e^k \chi_{S^c}) \quad (33)$$

$$= c(d(i, j) + d(j, k)). \quad (34)$$

□

Note that if the requirement (27) is dropped, it is easy to show that if  $d(i, j) = 0$  for some  $i \neq j$ , then  $d(i, k) = d(j, k)$  for *any*  $k$ . In this case the classes  $i$  and  $j$  can be collapsed into a single class as far as the regularizer is concerned. The decision between label  $i$  and  $j$  is then completely local, i.e. depends only on the data term and can be postponed to a post-processing step by modifying the data term to

$$s'_i(x) := s'_j(x) := \min\{s_i(x), s_j(x)\}. \quad (35)$$

Thus (27) is not a real limitation and can be always assured. As a side note, it can be shown that, under some assumptions and in the space of piecewise

constant functions, the subadditivity of  $d$  already follows if  $J$  is required to be lower semicontinuous [Bra02, p.88].

Proposition 1 implies that for non-metric  $d$ , we generally cannot expect to find a regularizer satisfying (P1)–(P3). Note that here  $J$  is not required to be of any particular form. In the following sections, we will show that on the other hand, if  $d$  is metric as in Proposition 1, such a regularizer can always be constructed. This implies that the interaction potentials allowing for a regularizer that satisfies (P1)–(P3) are exactly the metrics.

## 4 Constructing Regularizers from the Interaction Potential

We study next how to construct regularizers on  $BV(\Omega)^l$  satisfying (P1)–(P3). As in (25) we set

$$J(u) := \int_{\Omega} \Psi(Du). \quad (36)$$

We additionally require  $\Psi : \mathbb{R}^{d \times l} \rightarrow \mathbb{R}_{\geq 0}$  to be a support function, i.e. for some closed, convex  $\emptyset \neq \mathcal{D}_{\text{loc}} \subseteq \mathbb{R}^{d \times l}$ ,

$$\Psi(z) = \sigma_{\mathcal{D}_{\text{loc}}}(z) = \sup_{v(x) \in \mathcal{D}_{\text{loc}}} \langle z, v(x) \rangle. \quad (37)$$

As a support function,  $\Psi$  coincides with its recession function  $\Psi_{\infty}$ , thus

$$\begin{aligned} J(u) &= \int_{\Omega} \Psi(\mathcal{J}(u)(x)) dx + \dots \\ &\quad \int_{J_u} \Psi \left( \nu_u(x) (u^+(x) - u^-(x))^{\top} \right) d\mathcal{H}^{d-1} + \dots \\ &\quad \int_{\Omega} \Psi \left( \frac{D^c u}{|D^c u|} \right) d|D^c u|. \end{aligned} \quad (38)$$

Also, we have an equivalent dual formulation in analogy to (13),

$$J(u) = \sup \left\{ \int_{\Omega} \langle u, \text{Div } v \rangle dx \mid v \in C_c^{\infty}(\Omega)^{d \times l}, v(x) \in \mathcal{D}_{\text{loc}} \forall x \in \Omega \right\}. \quad (39)$$

For simplicity we will also assume that  $\mathcal{D}_{\text{loc}}$  is rotationally invariant along the image dimensions, i.e. for any rotation matrix  $R \in \mathbb{R}^{d \times d}$ ,

$$v = (v^1, \dots, v^l) \in \mathcal{D}_{\text{loc}} \Leftrightarrow (Rv^1, \dots, Rv^l) \in \mathcal{D}_{\text{loc}}. \quad (40)$$

This is equivalent to  $J$  being isotropic.

We will now show under which circumstances a minimizer exists in  $BV(\Omega)^l$ , and then see how the approach can be used to construct regularizers for specific interaction potentials.

### 4.1 Existence of Minimizers

The complete problem considered here is of the form (cf. (6) and (38))

$$\inf_{u \in \mathcal{C}} f(u), \quad f(u) := \int_{\Omega} \langle u, s \rangle dx + J(u) \quad (41)$$

where  $J(u) = \int_{\Omega} \Psi(Du)$  as in (36),

$$\Psi(z) = \sup_{v(x) \in \mathcal{D}_{\text{loc}}} \langle z, v(x) \rangle \quad (42)$$

for some closed convex  $\mathcal{D}_{\text{loc}} \neq \emptyset$ , and

$$\mathcal{C} = \{u \in \text{BV}(\Omega)^l \mid u(x) \in \Delta_l \mathcal{L}^d\text{-a.e. } x \in \Omega\}. \quad (43)$$

Note that  $f$  is convex, as it is the pointwise supremum of affine functions (39). Again for simplicity we set  $\Omega = (0, 1)^d$ . Then we have the following

**Proposition 2.** *Let  $\mathcal{D}_{\text{loc}} \neq \emptyset$  be closed convex,  $\Psi = \sigma_{\mathcal{D}_{\text{loc}}}$ ,  $s \in L^1(\Omega)^l$ , and*

$$f(u) = \int_{\Omega} \langle u, s \rangle dx + \int_{\Omega} \Psi(Du). \quad (44)$$

*Additionally assume that  $\mathcal{D}_{\text{loc}} \subseteq \mathcal{B}_{\rho_u}(0) \subseteq \mathbb{R}^{d \times l}$  for some  $0 < \rho_u$ . Then  $f$  is lower semicontinuous in  $\text{BV}(\Omega)^l$  with respect to  $L^1$  convergence.*

*Proof.* As the data term is continuous, it suffices to show that the regularizer is lower semicontinuous. This is an application of [AFP00, Thm. 5.47]. In fact, the theorem shows that  $f$  is the relaxation of  $\tilde{f} : C^1(\Omega)^l \rightarrow \mathbb{R}$ ,

$$\tilde{f}(u) := \int_{\Omega} \langle u, s \rangle dx + \int_{\Omega} \Psi(\mathcal{J}u(x)) dx, \quad (45)$$

on  $\text{BV}(\Omega)^l$  w.r.t.  $L^1_{\text{loc}}$  (thus here  $L^1$ ) convergence and thus lower semicontinuous in  $\text{BV}(\Omega)^l$ . To apply the theorem, we have to show that  $\Psi$  is quasiconvex in the sense of [AFP00, 5.25], which holds as it is convex by construction. The other precondition is (at most) linear growth of  $\Psi$ , which holds with  $0 \leq \Psi(x) \leq \rho_u \|x\|$ .  $\square$

**Proposition 3.** *Let  $f, \Psi, s$  as in Prop. 2 and additionally assume that*

$$\mathcal{B}_{\rho_l}(0) \cap \{(v^1, \dots, v^l) \mid \sum_i v^i = 0\} \subseteq \mathcal{D}_{\text{loc}} \subseteq \mathcal{B}_{\rho_u}(0) \quad (46)$$

*for some  $0 < \rho_l \leq \rho_u$ . Then the problem*

$$\min_{u \in \mathcal{C}} f(u) \quad (47)$$

*has at least one minimizer.*

*Proof.* From the inner and outer bounds it holds that  $\rho_l \|z\| \leq \Psi(z) \leq \rho_u \|z\|$  for any  $z = (z^1 \mid \dots \mid z^l) \in \mathbb{R}^{d \times l}$  with  $z^1 + \dots + z^l = 0$ . Moreover, the constraint  $u \in \mathcal{C}$  implies that  $Du = (Du_1 \mid \dots \mid Du_l)$  satisfies  $Du_1 + \dots + Du_l = 0$ . Combining this with the positive homogeneity of  $\Psi$ , it follows from (26) that

$$0 \leq \rho_l \text{TV}(u) \leq J(u) \leq \rho_u \text{TV}(u). \quad (48)$$

From

$$\int_{\Omega} \langle u, s \rangle dx \geq - \int_{\Omega} \|u(x)\|_{\infty} \|s(x)\|_1 dx, \quad (49)$$

the fact that  $s \in L^1(\Omega)^l$ , and boundedness of  $\Omega$  and  $\Delta_l$ , it follows that the data term is bounded from below on  $\mathcal{C}$ .

We now show coercivity of  $f$  with respect to the BV norm: Let  $(u^{(k)}) \subset \mathcal{C}$  with  $\|u^{(k)}\|_1 + \text{TV}(u^{(k)}) \rightarrow \infty$ . As the data term is bounded from below, and using the fact that  $J(u^{(k)}) \geq \rho_l \text{TV}(u^{(k)})$ , it follows that  $f(u^{(k)}) \rightarrow +\infty$ . Thus  $f$  is coercive.

Equations (48) and (49) also show that  $f$  is bounded from below. Thus we can choose a minimizing sequence  $(u^{(k)})$ . Due to the coercivity, the sequence  $\|u^{(k)}\|_1 + \text{TV}(u^{(k)})$  must then be bounded from above. From this and [AFP00, Thm. 3.23] we conclude that there is a subsequence of  $(u^{(k)})$  weakly\*- (and thus  $L^1$ -) converging to some  $u \in \text{BV}(\Omega)^l$ . With the lower semicontinuity from Prop. 2 and closedness of  $\mathcal{C}$  with respect to  $L^1$  convergence, existence of a minimizer follows.  $\square$

## 4.2 Relation to the Interaction Potential

To relate such  $J$  to the labeling problem in view of (P3), we have the following

**Proposition 4.** *Let  $\Psi = \sigma_{\mathcal{D}_{\text{loc}}}$  and  $J(u) = \int_{\Omega} \Psi(Du)$  as in Prop. 2. For some  $u' \in \text{BV}(\Omega)$  and vectors  $a, b \in \Delta_l$ , let  $u(x) = (1 - u'(x))a + u'(x)b$ . Then for any vector  $y \in \mathbb{R}^d$  with  $\|y\| = 1$ ,*

$$J(u) = \Psi(y(b-a)^{\top}) \text{TV}(u') = \left( \sup_{v \in \mathcal{D}_{\text{loc}}} \|v(b-a)\| \right) \text{TV}(u'). \quad (50)$$

*In particular, if  $\Psi(y(e^i - e^j)^{\top}) = d(i, j)$  for some  $y$  with  $\|y\| = 1$ , then  $J$  fulfills (P3).*

*Proof.* To show the first equality, (26) implies

$$J(u) = \int_{\Omega} \Psi \left( \frac{Du}{|Du|} \right) |Du| \quad (51)$$

$$= \int_{\Omega} \Psi \left( \frac{D(a + u'(b-a))}{|D(a + u'(b-a))|} \right) |D(a + u'(b-a))| \quad (52)$$

$$= \int_{\Omega} \Psi \left( \frac{(Du')(b-a)^{\top}}{|(Du')(b-a)^{\top}|} \right) |(Du')(b-a)^{\top}| \quad (53)$$

We make use of the property  $|(Du')(b-a)^{\top}| = |Du'| \|b-a\|$ , which is a direct consequence of the definition of the total variation measure and the fact that  $\|w(b-a)^{\top}\| = \|w\| \|b-a\|$  for any vector  $w \in \mathbb{R}^d$  (note that  $a, b \in \mathbb{R}^l$  are also vectors). Therefore

$$J(u) = \int_{\Omega} \Psi \left( \frac{(Du')(b-a)^{\top}}{|Du'| \|b-a\|} \right) |Du'| \|b-a\|, \quad (54)$$

which by positive homogeneity of  $\Psi$  implies

$$J(u) = \int_{\Omega} \Psi \left( \frac{Du'}{|Du'|} (b-a)^{\top} \right) |Du'|. \quad (55)$$

Since the density function  $Du'/|Du'|$  assumes values in  $S^{d-1}$ , there exists, for a.e.  $x \in \Omega$ , a rotation matrix mapping  $(Du'/|Du'|)(x)$  to  $y$ . Together with the

rotational invariance of  $\mathcal{D}_{\text{loc}}$  from (40) this implies

$$J(u) = \int_{\Omega} \Psi(y(b-a)^{\top}) |Du'| = \Psi(y(b-a)^{\top}) \text{TV}(u'), \quad (56)$$

which proves the first equality in (50). The second equality can be seen as follows:

$$r := \sup_{v \in \mathcal{D}_{\text{loc}}} \|v(b-a)\| \quad (57)$$

$$= \sup_{v \in \mathcal{D}_{\text{loc}}} \sup_{z \in \mathbb{R}^d, \|z\| \leq 1} \langle z, v(b-a) \rangle \quad (58)$$

$$= \sup_{z \in \mathbb{R}^d, \|z\| \leq 1} \sup_{v \in \mathcal{D}_{\text{loc}}} \langle z, v(b-a) \rangle. \quad (59)$$

Denote by  $R_z$  a rotation matrix mapping  $z$  to  $y$ , i.e.  $R_z z = y$ , then

$$r = \sup_{z \in \mathbb{R}^d, \|z\| \leq 1} \sup_{v \in \mathcal{D}_{\text{loc}}} \langle R_z z, R_z v(b-a) \rangle \quad (60)$$

$$= \sup_{z \in \mathbb{R}^d, \|z\| \leq 1} \sup_{v' \in R_z \mathcal{D}_{\text{loc}}} \langle y, v'(b-a) \rangle. \quad (61)$$

The rotational invariance of  $\mathcal{D}_{\text{loc}}$  provides  $R_z \mathcal{D}_{\text{loc}} = \mathcal{D}_{\text{loc}}$ , therefore

$$r = \sup_{z \in \mathbb{R}^d, \|z\| \leq 1} \sup_{v \in \mathcal{D}_{\text{loc}}} \langle y, v(b-a) \rangle \quad (62)$$

$$= \sup_{v \in \mathcal{D}_{\text{loc}}} \langle y, v(b-a) \rangle = \Psi(y(b-a)^{\top}). \quad (63)$$

□

As a consequence, if the relaxed multiclass formulation is restricted to two classes by parametrizing  $u = (1-u')a + u'b$  for  $u'(x) \in [0, 1]$ , it essentially reduces to the scalar continuous cut problem: Solving

$$\min_{\substack{u' \in \text{BV}(\Omega), \\ u'(x) \in [0, 1], \mathcal{L}^d\text{-a.e. } x \in \Omega}} \int_{\Omega} \langle (1-u')a + u'b, s \rangle dx + J(u) \quad (64)$$

is equivalent to solving

$$\min_{\substack{u' \in \text{BV}(\Omega), \\ u'(x) \in [0, 1], \mathcal{L}^d\text{-a.e. } x \in \Omega}} \int_{\Omega} u'(b-a) dx + \Psi(y(b-a)^{\top}) \text{TV}(u') \quad (65)$$

which is just the classical binary continuous cut approach with data  $(b-a)$  and regularizer weight  $\Psi(y(b-a)^{\top})$ , where  $y \in \mathbb{R}^d$  is some arbitrary unit vector. For the multiclass case, assume that

$$u = u_P = e^1 \chi_{P^1} + \dots + e^l \chi_{P^l} \quad (66)$$

for some partition  $P^1 \cup \dots \cup P^l = \Omega$  with  $\text{Per}(P^i) < \infty, i = 1, \dots, l$ . Then the absolutely continuous and Cantor parts vanish [AFP00, Thm. 3.59, Thm. 3.84, Rem. 4.22], and only the jump part remains:

$$J(u_P) = \int_{S_{u_P}} \Psi\left(\nu_{u_P}(u_{P^+} - u_{P^-})^{\top}\right) d\mathcal{H}^{d-1}, \quad (67)$$



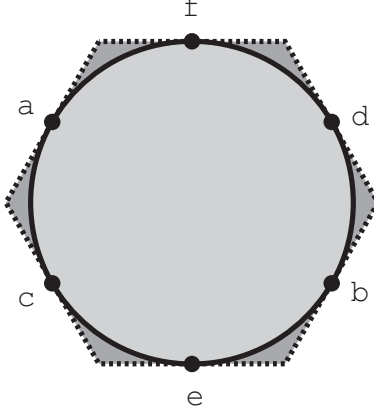


Figure 5: Illustration of the set  $\mathcal{D}_{\text{loc}}$  used to build the regularizer for the uniform distance,  $d(i, j) = 0$  iff  $i = j$  and  $d(i, j) = 1$  otherwise, for  $l = 3$  and  $d = 1$ , i.e. in a one-dimensional space. Shown is a cut through the  $z^1 + z^2 + z^3 = 0$  plane; the labels correspond to the points  $e^i - e^j$  with  $i \neq j$ . The local envelope method leads to a larger set  $\mathcal{D}_{\text{loc}}$  (dashed) than the Euclidean metric method (solid). This improves the tightness of the relaxation, but requires more expensive projection steps.

where  $S_{u_P} = \bigcup_{i=1, \dots, l} \partial P^i$  is the union of the interfaces between regions. Define  $i(x), j(x)$  such that  $u_{P+}(x) = e^{i(x)}$  and  $u_{P-}(x) = e^{j(x)}$ . Then

$$J(u_P) = \int_{S_{u_P}} \Psi \left( \nu_{u_P} \left( e^{i(x)} - e^{j(x)} \right)^\top \right) d\mathcal{H}^{d-1}. \quad (68)$$

By rotational invariance,

$$J(u_P) = \int_{S_{u_P}} \Psi \left( y \left( e^{i(x)} - e^{j(x)} \right)^\top \right) d\mathcal{H}^{d-1}. \quad (69)$$

for some  $y$  with  $\|y\| = 1$ . Thus the regularizer locally penalizes jumps between labels  $i$  and  $j$  along an interface with the interface length, multiplied by the factor  $\Psi(y(e^i - e^j)^\top)$  depending on the labels of the adjoining regions.

The question is how to choose the set  $\mathcal{D}_{\text{loc}}$  such that  $\Psi(y(e^i - e^j)^\top) = d(i, j)$  for a given interaction potential  $d$ . We will consider two approaches which differ with respect to expressiveness and simplicity of use: In the *local envelope* approach (Sect. 4.3),  $\mathcal{D}_{\text{loc}}$  is chosen as large as possible. In turn,  $J$  is as large as possible with the integral formulation (36). This prevents introducing artificial minima generated by the relaxation, and potentially keeps minimizers of the relaxed problem close to minimizers of the discrete problem. However,  $\mathcal{D}_{\text{loc}}$  is only implicitly defined, which complicates optimization. In contrast, in the *embedding* approach (Sect. 4.4),  $\mathcal{D}_{\text{loc}}$  is simpler at the cost of being able to represent only a subset of all metric potentials  $d$ . For an illustration of the two approaches, see Fig. 5.

### 4.3 Local Envelope Method

Chambolle et al. [CCP08] proposed an interesting approach for potentials  $d$  of the form  $d(i, j) = \gamma(|i - j|)$  for a positive concave function  $\gamma$ . The approach is derived by specifying the value of  $J$  on discrete  $u$  only and then constructing an approximation of the convex envelope by pulling the convexification into the integral. This potentially generates tight extensions and thus one may hope that the convexification process does not generate too many artificial non-discrete solutions.

We propose to extend this approach to *arbitrary metric*  $d$  by setting (Fig. 5)

$$\mathcal{D}_{\text{loc}}^d := \bigcap_{i \neq j} \{v = (v^1, \dots, v^l) \in \mathbb{R}^{d \times l} \mid \|v^i - v^j\| \leq d(i, j), \sum_k v^k = 0\} \quad (70)$$

for some given interface potential  $d(i, j)$ . By definition  $\mathcal{D}_{\text{loc}}^d$  is rotationally invariant, and by the considerations in Sect. 3 we assume  $d$  to be a metric. Then the inner and outer bound assumptions required for existence of a minimizer in Prop. 3 are satisfied. Moreover,  $d$  can be reconstructed from  $\mathcal{D}_{\text{loc}}^d$ :

**Proposition 5.** *Let  $d : \{1, \dots, l\}^2 \rightarrow \mathbb{R}_{\geq 0}$  be a metric. Then for any  $i, j$ ,*

$$\sup_{v \in \mathcal{D}_{\text{loc}}^d} ((v^i)_1 - (v^j)_1) = d(i, j). \quad (71)$$

*Proof.* “ $\leq$ ” follows from the definition (70). “ $\geq$ ” can be shown using a network flow argument: We have

$$\sup_{v \in \mathcal{D}_{\text{loc}}^d} ((v^i)_1 - (v^j)_1) \quad (72)$$

$$\geq \sup\{p_i - p_j \mid p \in \mathbb{R}^l, \sum_k p_k = 0, \forall i', j' : p_{i'} - p_{j'} \leq d(i', j')\} \quad (73)$$

$$\stackrel{(*)}{=} \sup\{p_i - p_j \mid p \in \mathbb{R}^l, \forall i', j' : p_{i'} - p_{j'} \leq d(i', j')\} \quad (74)$$

$$\stackrel{(**)}{=} d(i, j). \quad (75)$$

Equality  $(*)$  holds since each  $p$  in the set in (74) can be associated with  $\tilde{p} := p - \frac{1}{l} \sum_k p_k$ , which is contained in the set in (73) and satisfies  $p_i - p_j = \tilde{p}_i - \tilde{p}_j$ . The last equality  $(**)$  follows from [Mur03, 5.1] with the notation  $\gamma = d$  (and  $\bar{\gamma} = d$ , since  $d$  is a metric and therefore the triangle inequality implies that the length of the shortest path from  $i$  to  $j$  is always  $d(i, j)$ ).  $\square$

The final result of this section is the following:

**Proposition 6.** *Let  $d : \mathbb{R}^{l \times l} \rightarrow \mathbb{R}_{\geq 0}$  be a metric. Define  $\mathcal{D}_{\text{loc}} := \mathcal{D}_{\text{loc}}^d$  as in (70),  $\Psi_d := \sigma_{\mathcal{D}_{\text{loc}}^d}$  and*

$$J_d := \int_{\Omega} \Psi_d(Du) \quad (76)$$

*as in (38). Then  $J_d$  satisfies (P1)–(P3).*

*Proof.* (P1) and (P2) are clear from the definition of  $J_d$ . (P3) follows directly from Prop. 5 and Prop. 4 with  $y = e^1$ .  $\square$

Defining  $\mathcal{D}_{\text{loc}}^d$  as in (70) provides us with a way to extend the desired regularizer for *any* metric  $d$  to non-discrete  $u \in \mathcal{C}$  via (38). The price to pay is that there is no simple closed expression for  $\Psi$  and thus for  $J_d$ , which potentially complicates optimization. Note that in order to define  $\mathcal{D}_{\text{loc}}^d$ ,  $d$  does not have to be a metric. However Prop. 5 then does not hold in general, so  $J$  is not a true extension of the desired regularizer, although it still provides a lower bound.

#### 4.4 Euclidean Metric Method

In this section, we consider a regularizer which is less powerful but more efficient to evaluate. The classical total variation for vector-valued  $u$  as defined in (13) is

$$\text{TV}(u) = \int_{\Omega} \|Du\|. \quad (77)$$

This classical definition has also been used in color denoising and is also referred to as MTV [SR96, DAV08]. We propose to extend this definition by choosing an *embedding matrix*  $A \in \mathbb{R}^{k \times l}$  for some  $k \leq l$ , and defining

$$J_A(u) := \text{TV}(Au). \quad (78)$$

This corresponds to substituting the Frobenius matrix norm on the distributional gradient with a linearly weighted variant. In the framework of (38), it amounts to setting  $\mathcal{D}_{\text{loc}} = \mathcal{D}_{\text{loc}}^A$  (cf. Fig. 5) with

$$\mathcal{D}_{\text{loc}}^A := \{v'A | v' \in \mathbb{R}^{d \times k}, \|v'\| \leq 1\} = \mathcal{B}_1(0)A \quad (79)$$

Clearly,  $0 \in \mathcal{D}_{\text{loc}}^A$  and

$$\Psi(z) = \sigma_{\mathcal{D}_{\text{loc}}^A}(z) = \sup_{v' \in \mathcal{B}_1(0)A} \langle z, v' \rangle = \sup_{v \in \mathcal{B}_1(0)} \langle z, vA \rangle \quad (80)$$

$$= \sup_{v \in \mathcal{B}_1(0)} \langle zA^\top, v \rangle = \|zA^\top\|. \quad (81)$$

In particular, we formally have

$$\Psi(Du) = \|(Du)A^\top\| = \|D(Au)\|, \quad (82)$$

as  $u \mapsto Du$  is linear in  $u$ . To clarify the definition, we may rewrite this to

$$\text{TV}_A(u) = \int_{\Omega} \sqrt{\|D_1 u\|_A^2 + \dots + \|D_d u\|_A^2}, \quad (83)$$

where  $\|v\|_A := (v^\top A^\top A v)^{1/2}$ . In this sense, the approach can be understood as replacing the Euclidean norm by a linearly weighted variant.

It remains to show for which interaction potentials  $d$  assumption (P3) can be satisfied. The next proposition shows that this is possible for the class of *Euclidean* metrics.

**Proposition 7.** *Let  $d$  be an Euclidean metric, i.e. there exist  $k \in \mathbb{N}$  as well as  $a^1, \dots, a^l \in \mathbb{R}^k$  such that  $d(i, j) = \|a^i - a^j\|$ . Then for  $A = (a^1 | \dots | a^l)$ ,  $J_A := \text{TV}_A$  satisfies (P1)–(P3).*

*Proof.* (P1) and (P2) are clearly satisfied. In order to show (P3) we apply Prop. 4 and assume  $\|y\| = 1$  to obtain with (81)

$$\begin{aligned}\Psi(y(e^i - e^j)^\top) &= \|y(e^i - e^j)^\top A^\top\| \\ &= \|y(a^i - a^j)^\top\| = \|a^i - a^j\|.\end{aligned}\tag{84}$$

□

The class of Euclidean metrics comprises some important special cases:

- The *uniform*, *discrete* or *Potts* metric as also considered in [ZGFN08, LKY<sup>+</sup>09] and as a special case in [KT99, KT07]. Here  $d(i, j) = 0$  iff  $i = j$  and  $d(i, j) = 1$  in any other case, which corresponds to  $A = (1/\sqrt{2})I$ .
- The *linear* (label) metric,  $d(i, j) = c|i - j|$ , with  $A = (c, 2c, \dots, lc)$ . This regularizer is suitable to problems where the labels can be naturally ordered, e.g. depth from stereo or grayscale image denoising.
- More generally, if label  $i$  corresponds to a prototypical vector  $z^i$  in  $k$ -dimensional feature space, and the Euclidean norm is an appropriate metric on the features, it is natural to set  $d(i, j) = \|z^i - z^j\|$ , which is Euclidean by construction. This corresponds to a regularization in feature space, rather than in “label space”.

Note that the boundedness assumption involving  $\rho_l$  required for the existence proof (Prop. 3) is only fulfilled if the kernel of  $A$  is sufficiently small, i.e.  $\ker A \subseteq \{te | t \in \mathbb{R}\}$ , with  $e = (1, \dots, 1)^\top \in \mathbb{R}^l$ : Otherwise,  $\mathcal{D}_{\text{loc}}^A = (\mathcal{B}_1(0)A) \cap \{(v^1, \dots, v^l) | \sum_i v^i = 0\}$  is contained in a subspace of at most dimension  $(l-2)d$ , and (46) cannot be satisfied for any  $\rho_l > 0$ . Thus if  $d$  is a degenerate Euclidean metric which can be represented by an embedding into a lower-dimensional space, as is the case with the linear metric, it has to be regularized for the existence result in Prop. 3 to hold. This can for example be achieved by choosing an orthogonal basis  $(b^1, \dots, b^j)$  of  $\ker A$ , where  $j = \dim \ker A$ , and substituting  $A$  with  $A' := (A^\top, \varepsilon b^1, \dots, \varepsilon b^j)^\top$ , enlarging  $k$  as required. However these observations are mostly of theoretical interest, as the existence of minimizers for the discretized problem follows already from compactness of the (finite-dimensional) discretized constraint set.

Non-Euclidean  $d$ , such as the *truncated linear metric*,  $d(i, j) = \min\{2, |i - j|\}$ , cannot be represented exactly by  $\text{TV}_A$ . In the following we will demonstrate how to construct approximations for these cases.

Assume that  $d$  is an arbitrary metric with squared matrix representation  $D \in \mathbb{R}^{l \times l}$ , i.e.  $D_{ij} = d(i, j)^2$ . Then it is known [BG05] that  $d$  is Euclidean iff for  $C := I - \frac{1}{l}ee^\top$ , the matrix  $T := -\frac{1}{2}CDC$  is positive semidefinite. In this case,  $d$  is called *Euclidean distance matrix*, and  $A$  can be found by factorizing  $T = A^\top A$ . If  $T$  is not positive semidefinite, setting the nonnegative eigenvalues in  $T$  to zero yields an Euclidean approximation. This method is known as *classical scaling* [BG05] and does not necessarily give good absolute error bounds.

More generally, for some non-metric, nonnegative  $d$ , we can formulate the problem of finding the “closest” Euclidean distance matrix  $E$  as the minimization problem of a matrix norm  $\|E - D\|_M$  over all  $E \in \mathcal{E}_l$ , the set of  $l \times l$  Euclidean distance matrices. Fortunately, there is a linear bijection  $B : \mathcal{P}_{l-1} \rightarrow \mathcal{E}_l$  between  $\mathcal{E}_l$  and the space of positive semidefinite  $(l-1) \times (l-1)$  matrices  $\mathcal{P}_{l-1}$

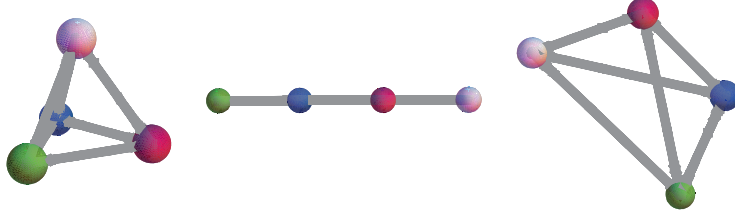


Figure 6: Euclidean embeddings into  $\mathbb{R}^3$  for several interaction potentials with four classes. **Left to right:** Potts; linear metric; non-Euclidean truncated linear metric. The vertices correspond to the columns  $a^1, \dots, a^l$  of the embedding matrix  $A$ . For the truncated linear metric an optimal approximate embedding was computed as outlined in Sect. 4.4 with the matrix norm  $\|X\|_M := \max_{i,j} |X_{ij}|$ .

[Gow85, JT95]. This allows us to rewrite our problem as a *semidefinite program* [WSV00, (p.534–541)]

$$\inf_{S \in \mathcal{P}_{l-1}} \|B(S) - D\|_M. \quad (85)$$

Problem (85) can be solved using available SDP solvers. Then  $E = B(S) \in \mathcal{E}_l$ , and  $A$  can be extracted by factorizing  $-\frac{1}{2}CEC$ . Since both  $E$  and  $D$  are explicitly known,  $\varepsilon_E := \max_{i,j} |(E_{ij})^{1/2} - (D_{ij})^{1/2}|$  can be explicitly computed and provides an a posteriori bound on the maximum distance error. Fig. 6 shows a visualization of some embeddings for a four-class problem. In many cases, in particular when the number of classes is large, the Euclidean embedding provides a good approximation for non-Euclidean metrics (Fig. 7).

Based on the embedding matrices computed in this way, the Euclidean distance approach can be used to solve approximations of the labeling problem with arbitrary metric interaction potentials, with the advantage of having a closed expression for the regularizer.

## 5 Discretized Problem

### 5.1 Saddle Point Formulation

We now turn to solving the discretization of the relaxed problem (41). In order to formulate generic algorithms, we study the bilinear saddle point problem,

$$\min_{u \in \mathcal{C}} \max_{v \in \mathcal{D}} g(u, v), \quad g(u, v) := \langle u, s \rangle + \langle Lu, v \rangle - \langle b, v \rangle. \quad (86)$$

As will be shown in Sect. 5.2–5.4, this covers both  $J_d$  (76) and  $J_A$  (78) as well as many other – even non-uniform and non-isotropic – regularizers.

In a slight abuse of notation, we will denote by  $u, s \in \mathbb{R}^n$  also the discretizations of  $u$  and  $s$  on a uniform grid. Furthermore we require a linear operator  $L \in \mathbb{R}^{m \times n}$ , a vector  $b \in \mathbb{R}^m$  for some  $m, n \in \mathbb{N}$ , and bounded closed convex sets  $\mathcal{C} \subseteq \mathbb{R}^n, \mathcal{D} \subseteq \mathbb{R}^m$ . Intuitively,  $L$  discretizes the gradient operator and  $\mathcal{D}$  corresponds to  $\mathcal{D}_{\text{loc}}$ , i.e. specifies  $\Psi$  in a dual formulation. The primal and dual objectives are

$$f(u) := \max_{v \in \mathcal{D}} g(u, v) \quad \text{and} \quad f_D(v) := \min_{u \in \mathcal{C}} g(u, v), \quad (87)$$

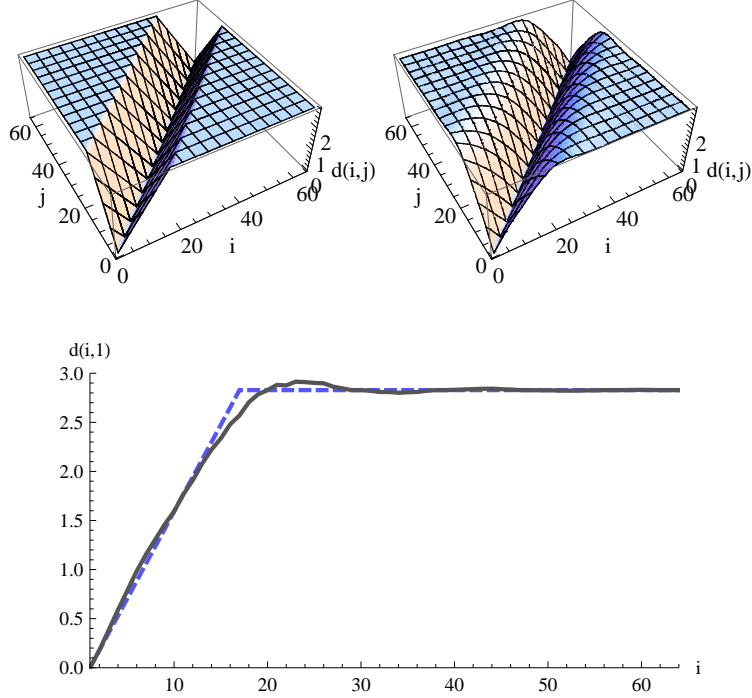


Figure 7: Euclidean approximation of the Non-Euclidean truncated linear metric with interaction potential  $d(i, j) = \sqrt{2}/8 \min\{|i - j|, 16\}$ . **Left to Right:** Original potential for 64 classes; potential after Euclidean approximation. **Bottom:** cross section of the original (dashed) and approximated (solid) metric at  $i = 1$ . The approximation was computed using semidefinite programming as outlined in Sect. 4.4. It represents the closest Euclidean metric with respect to the matrix norm  $\|X - Y\|_M := \sum_{i,j} |X_{ij} - Y_{ij}|$ . The maximal error with respect to the original potential is  $\varepsilon_E = 0.2720$ .

respectively. The dual problem then consists of maximizing  $f_D(v)$  over  $\mathcal{D}$ . As  $\mathcal{C}$  and  $\mathcal{D}$  are bounded, it follows from [Roc70, Cor. 37.6.2] that a saddle point  $(u^*, v^*)$  of  $g$  exists. With [Roc70, Lemma 36.2], this implies strong duality, i.e.

$$\min_{u \in \mathcal{C}} f(u) = f(u^*) = g(u^*, v^*) = f_D(v^*) = \max_{v \in \mathcal{D}} f_D(v). \quad (88)$$

In our case,  $\mathcal{C}, \mathcal{D}$  exhibit a specific product structure, which allows to compute  $f_D$  as well as the orthogonal projections  $\Pi_{\mathcal{C}}$  and  $\Pi_{\mathcal{D}}$  efficiently, a fact that will prove important in the algorithmic part. The evaluation of the primal objective  $f$  on the other hand can be more difficult, depending on the definition of  $\mathcal{D}_{\text{loc}}$  resp.  $\mathcal{D}$ , but is not required by the optimizer. Note that in the discrete framework, we may easily substitute non-homogeneous, spatially varying or even nonlocal regularizers by choosing  $L$  and  $b$  appropriately.

---

**Algorithm 1** Projection of  $y \in \mathbb{R}^l$  onto the standard simplex  $\Delta_l$

---

```

1:  $Z^{(0)} \leftarrow \emptyset, y^{(0)} \leftarrow y \in \mathbb{R}^l, k \leftarrow 0.$ 
2: repeat
3:    $\tilde{y}_i^{(k+1)} \leftarrow \begin{cases} 0, & i \in Z^{(k)}, \\ y_i^{(k)} - \frac{e^\top y^{(k)}}{l - |Z^{(k)}|}, & \text{otherwise,} \end{cases} \quad (i = 1, \dots, l).$ 
4:    $Z^{(k+1)} \leftarrow \{i \in \{1, \dots, l\} | i \in Z^{(k)} \text{ or } \tilde{y}_i^{(k+1)} < 0\}.$ 
5:    $y_i^{(k+1)} \leftarrow \max\{\tilde{y}_i^{(k+1)}, 0\} \quad (i = 1, \dots, l).$ 
6:    $k \leftarrow k + 1.$ 
7: until  $\tilde{y}^{(k+1)} \geq 0.$ 

```

---

## 5.2 Discretization

We discretize  $\Omega$  by a regular grid,  $\Omega = \{1, \dots, n_1\} \times \dots \times \{1, \dots, n_d\} \subseteq \mathbb{R}^d$  for  $d \in \mathbb{N}$ , consisting of  $n := |\Omega|$  pixels  $(x^1, \dots, x^n)$  in lexicographical order. We represent  $u$  by its values  $u = (u^1 | \dots | u^l) \in \mathbb{R}^{n \times l}$  at these points, and denote by  $u^{x^j} \in \mathbb{R}^l, j = 1, \dots, n$ , the  $j$ -th row of  $u$ , corresponding to  $u(x^j)$ . The multidimensional image space  $\mathbb{R}^{n \times l}$  is equipped with the Euclidean inner product  $\langle \cdot, \cdot \rangle$  over the vectorized elements. We identify  $u \in \mathbb{R}^{n \times l}$  with the vector in  $\mathbb{R}^{nl}$  obtained by concatenating the columns.

Let  $\text{grad} := (\text{grad}_1^\top | \dots | \text{grad}_d^\top)^\top$  be the  $d$ -dimensional forward differences gradient operator for Neumann boundary conditions. Then  $\text{div} := -\text{grad}^\top$  is the backward differences divergence operator for Dirichlet boundary conditions. These operators extend to  $\mathbb{R}^{n \times l}$  via  $\text{Grad} := (I_l \otimes \text{grad})$ ,  $\text{Div} := (I_l \otimes \text{div})$ . We define, for some  $k \geq 1$  as will be specified below, the convex sets

$$\mathcal{C} := \{u \in \mathbb{R}^{n \times l} | u^{x^j} \in \Delta_l, j = 1, \dots, n\}, \quad (89)$$

$$\mathcal{D} := \prod_{x \in \Omega} \mathcal{D}_{loc} \subseteq \mathbb{R}^{n \times d \times k}. \quad (90)$$

The set  $\mathcal{D}_{loc}$  and the operator  $L$  depend on the chosen regularizer. Note that for  $L := \text{Grad}$ ,  $k = l$  and

$$\mathcal{D}_{loc} := \mathcal{D}_{loc}^l := \{p = (p^1 | \dots | p^l) \in \mathbb{R}^{d \times l} | \|p\| \leq 1\}, \quad (91)$$

the primal objective in the saddle point formulation discretizes the classical vector-valued total variation,

$$\text{TV}(u) := \sigma_{\text{Div } \mathcal{D}}(u) = \sigma_{\mathcal{D}}(\text{Grad } u) = \sum_{j=1}^n \|G_{x^j} u\|, \quad (92)$$

where each of the  $G_{x^j}$  is an  $(ld) \times (nl)$  matrix composed of rows of  $(\text{Grad})$  such that  $G_{x^j} u$  constitutes the vectorized discrete Jacobian of  $u$  at the point  $x^j$ .

Projections on the set  $\mathcal{C}$  are highly separable and can be computed exactly in a finite number of steps [Mic86, Alg. 4], see Alg. 1 for a summary of the pointwise operation. The dual objective is

$$f_D(v) = -\langle b, v \rangle + \min_{u \in \mathcal{C}} \langle u, L^\top v + s \rangle. \quad (93)$$

Since the minimum decouples spatially, and  $\min_{y \in \Delta_l} \langle y, z \rangle = \text{vecmin}(z) := \min_i z_i$  for all  $z \in \mathbb{R}^l$ , the dual objective can always be evaluated by summing,

over all points  $x \in \Omega$ , the minima over the components of  $L^\top v + s$  corresponding to each point, denoted by  $(L^\top v + s)_{x^j}$ ,

$$f_D(v) = -\langle b, v \rangle + \sum_{j=1}^n \text{vecmin}((L^\top v + s)_{x^j}) . \quad (94)$$

This fact is helpful if evaluating the primal objective is costly because the dual set  $\mathcal{D}_{\text{loc}}$  has a complicated structure.

### 5.3 Specialization for the Local Envelope Method

For a metric interaction potential  $d : \{1, \dots, l\}^2 \rightarrow \mathbb{R}_{\geq 0}$ , we set  $k := l$  and

$$\begin{aligned} L &:= \text{Grad} , \\ \mathcal{D}_{\text{loc}} &:= \mathcal{D}_{\text{loc}}^d = \bigcap_{i \neq j} \{v = (v^1 | \dots | v^l) \in \mathbb{R}^{d \times l} \mid \|v^i - v^j\| \leq d(i, j)\} \end{aligned} \quad (95)$$

as in (70). We arrive at the saddle point form (86) with  $\mathcal{C}$ ,  $\mathcal{D}$ , and  $L$  defined as above,  $m = nl$  and  $b = 0$ . However due to the generality of the regularizer (cf. Prop. 6), the primal objective  $f$  cannot be easily computed anymore (for the special case of three labels there is a derivation in [CCP08]). Projections on  $\mathcal{D}$  can be computed for all  $x \in \Omega$  in parallel, while projections on the individual sets  $\mathcal{D}_{\text{loc}}^d$  can be computed by the Dykstra algorithm, cf. [CCP08] and Sect. 6.4.

### 5.4 Specialization for the Euclidean Metric Method

For  $A \in \mathbb{R}^{k \times l}$  as in (78), the Euclidean regularizer can be obtained by setting

$$\begin{aligned} L &:= (\text{Grad})(A \otimes I_n) , \\ \mathcal{D}_{\text{loc}} &:= \mathcal{D}_{\text{loc}}^I = \{v = (v^1 | \dots | v^k) \in \mathbb{R}^{d \times k} \mid \|v\| \leq 1\} . \end{aligned} \quad (96)$$

Departing from the definition (79) of  $\mathcal{D}_{\text{loc}}^A$ ,  $A$  is merged into  $L$ , as the optimization method will rely on projections on  $\mathcal{D}_{\text{loc}}$ . Including  $A$  into  $\mathcal{D}_{\text{loc}}$ , i.e. by setting

$$\mathcal{D}_{\text{loc}} := (A \otimes I_n)^\top \mathcal{D}_{\text{loc}}^I \quad (97)$$

and  $L := \text{Grad}$ , would prevent computing the projection in closed form. Projecting on the unit ball  $\mathcal{D}_{\text{loc}}^I$  on the other hand is trivial. The discretized regularizer can be explicitly evaluated, since

$$\Psi(z) = \|zA^\top\| . \quad (98)$$

Comparison to (92) yields

$$J_A(u) = \text{TV}((A \otimes I_n)u) . \quad (99)$$

We finally arrive at the form (86) with  $\mathcal{C}$ ,  $\mathcal{D}$ , and  $L$  defined as above,  $m = nk$  and  $b = 0$ . Projections on  $\mathcal{D}$  are highly separable and thus can be computed easily. The primal objective can be evaluated in closed form using (99).



## 5.5 Optimality

If  $f_D$  and  $f$  can be explicitly computed, any  $v \in \mathcal{D}$  provides an optimality bound on the primal objective, with respect to the optimal value  $f(u^*)$ , via the numerical *primal-dual gap*  $f(u) - f_D(v)$ ,

$$0 \leq f(u) - f(u^*) \leq f(u) - f_D(v). \quad (100)$$

Assuming  $f$  and  $f_D$  can be evaluated, the gap is a convenient stopping criterion. To improve the scale invariance, it is often practical to stop on the *relative gap*

$$\frac{f(u) - f_D(v)}{f_D(v)} \quad (101)$$

instead, which gives a similar bound. However convergence in the objective alone does not necessarily imply convergence in  $u$ , as the minimizer of the original problem (86) is generally not unique. This stands in contrast to the well-known ROF-type problems [ROF92], where the uniqueness is induced by a quadratic data term.

For some applications, after solving the relaxed problem a discrete solution – or “hard” labeling – still needs to be recovered, i.e. the relaxed solution needs to be *binarized*. For the continuous two-class case with the classical TV regularizer, [CEN06] showed that an exact solution can be obtained by thresholding at almost any threshold. However, their results do not seem to transfer to the multi-class case.

Another difficulty lies in the discretization: In order to apply the thresholding theorem, a crucial “coarea”-like property must hold for the *discretized* problem [CD09], which holds for the graph-based pairwise  $\ell_1$ -, but not the higher order  $\ell_2$ -discretization of the TV. Thus, even in the two-class case, simple thresholding may lead to a suboptimal discrete solution.

Currently we are not aware of an a priori bound on the error introduced by the binarization step in the general case. In practice, any dual feasible point together with (100) yields an a posteriori optimality bound: Let  $u^{(N)}, v^{(N)}$  be a pair of primal resp. dual feasible iterates,  $\bar{u}^{(N)}$  the result of the binarization step applied to  $u^{(N)}$ , and  $\bar{u}^*$  the optimal discrete solution. Then  $\bar{u}^{(N)}$  is primal feasible, and its suboptimality with respect to the optimal discrete solution is bounded from above by

$$f(\bar{u}^{(N)}) - f(\bar{u}^*) \leq f(\bar{u}^{(N)}) - f(u^*) \leq f(\bar{u}^{(N)}) - f_D(v^{(N)}). \quad (102)$$

Computation of  $f_D$ , and in many cases also  $f$ , is efficient as outlined in Sect. 5.2.

## 5.6 Improving the Binarization

There seems to be no obvious best choice for the binarization step. The simplest choice is the *first-max* approach: the label  $\ell(x)$  is set to the index of the first maximal component of the relaxed solution  $\bar{u}^{(N)}(x)$ . However, this might lead to undesired side effects: Consider the segmentation of a grayscale image with the three labels 1, 2, 3 corresponding to the gray level intensity, together with the linear distance  $d(i, j) = |i - j|$ , which is exactly representable using the Euclidean distance approach with  $A = (1 \ 2 \ 3)$ . Assume there is a region where  $\bar{u}^{(N)} = (1/3 + \delta(x), 1/3, 1/3 - \delta(x))$  for some small noise  $\delta(x) \in \mathbb{R}$ . The most

“natural” choice given the interpretation as grayscale values is the constant labeling  $\ell(x) = 2$ . The first-max approach gives  $\ell(x) \in \{1, 3\}$ , depending on the sign of  $\delta(x)$ , which leads to a noisy final segmentation.

On closer inspection, the first-max approach – which works well for the Potts distance – corresponds to choosing

$$\ell(x) = \arg \min_{\ell \in \{1, \dots, l\}} \|u(x) - e^\ell\|, \quad (103)$$

with the smallest  $\ell$  chosen in case of ambiguity. We propose to extend this to non-uniform distances by setting

$$\begin{aligned} \ell(x) &= \arg \min_{\ell \in \{1, \dots, l\}} \bar{\Psi}(u(x) - e^\ell), \\ \bar{\Psi} : \mathbb{R}^l &\rightarrow \mathbb{R}, \bar{\Psi}(z) := \Psi(e^1 z^\top). \end{aligned} \quad (104)$$

That is, we select the label corresponding to the nearest unit vector *with respect to*  $\bar{\Psi}$  (note that instead of  $e^1$  we could choose any normalized vector as  $\Psi$  is assumed to be rotationally invariant). In fact, for the linear distance example above we have  $\bar{\Psi}(z) = |-z_1 + z_3|$ . Thus

$$\begin{aligned} \bar{\Psi}(u(x) - e^1) &= |1 - 2\delta(x)|, \\ \bar{\Psi}(u(x) - e^2) &= |2\delta(x)|, \\ \bar{\Psi}(u(x) - e^3) &= |1 + 2\delta(x)|, \end{aligned} \quad (105)$$

and for small  $\delta$  we will get the stable and semantically correct choice  $\ell(x) = 2$ . This method proved to work well in practice, and considerably reduced the suboptimality introduced by the binarization step (Sect. 7.5). In case there is no closed form expression of  $\Psi$ , it can be numerically approximated as outlined in Sect. 6.5.

## 6 Optimization

When optimizing the saddle point problem (86), one must take care of its large-scale nature and the inherent nonsmoothness of the objective. While interior-point solvers are known to be very fast for small to medium sized problems, they are not particularly suited well for massively parallel computation, such as on the upcoming GPU platforms, due to the expensive inner Newton iterations.

We will instead focus on *first order* methods involving only basic operations that can be easily parallelized due to their local nature, such as evaluations of  $L$  and  $L^\top$  and projections on  $\mathcal{C}$  and  $\mathcal{D}$ . The first two methods are stated here for comparison, the third one is new. It additionally requires evaluating  $(I + L^\top L)^{-1}$ , which is potentially non-local, but in many cases can still be computed fast and explicitly using the Discrete Cosine Transform as shown below.

The following approaches rely on computing projections on the full sets  $\mathcal{D}$  resp.  $\mathcal{D}_{\text{loc}}$ , which requires an iterative procedure for non-trivial constraint sets such as obtained when using the local envelope method (Sect. 6.4). We would like to mention that by introducing further auxiliary variables and a suitable splitting approach, these inner iterations can also be avoided [LBS10]. However the number of additional variables grows quadratically in the number of labels,

---

**Algorithm 2** FPD Multi-Class Labeling

---

```
1: Choose  $\bar{u}^{(0)} \in \mathbb{R}^{n \times l}, v^{(0)} \in \mathbb{R}^{n \times d \times l}$ .
2: Choose  $\tau_P > 0, \tau_D > 0, N \in \mathbb{N}$ .
3: for  $k = 0, \dots, N - 1$  do
4:    $v^{(k+1)} \leftarrow \Pi_D (v^{(k)} + \tau_D (L\bar{u}^{(k)} - b))$ .
5:    $u^{(k+1)} \leftarrow \Pi_C (u^{(k)} - \tau_P (L^\top v^{(k+1)} + s))$ .
6:    $\bar{u}^{(k+1)} \leftarrow 2u^{(k+1)} - u^{(k)}$ .
7: end for
```

---

therefore the approach is only feasible for relatively small numbers of labels and memory requirements are usually one to several orders of magnitude higher than for the approaches discussed next.

### 6.1 Fast Primal-Dual Method

One of the most straightforward approaches for optimizing (86) is to fix small primal and dual step sizes  $\tau_P$  resp.  $\tau_D$ , and alternately apply projected gradient descent resp. ascent on the primal resp. dual variables. This *Arrow-Hurwicz* approach [AHU64] was proposed in a PDE framework for solving the two-class labeling problem in [AT06] and recently used in [CCP08]. An application to denoising problems can be found in [ZC08]. However it seems nontrivial to derive sufficient conditions for convergence. Therefore in [PCBC09a] the authors propose the *Fast Primal-Dual* (FPD) method, a variant of Popov's saddle point method [Pop80] with provable convergence. The algorithm is summarized in Alg. 2.

Due to the explicit steps involved, there is an upper bound condition on the step size to assure convergence, which can be shown to be  $\tau_P \tau_D < 1/\|L\|^2$  [PCBC09a]. The operator norm can be bounded according to

$$\|L\| \leq \|\text{Grad}\| \leq 2\sqrt{d} \quad (106)$$

for the envelope method, and

$$\|L\| \leq \|\text{Grad}\| \|A\| \leq 2\sqrt{d} \|A\| \quad (107)$$

for the Euclidean metric method. As both the primal and dual iterates are always feasible due to the projections, a stopping criterion based on the primal-dual gap as outlined in Sect. 5.5 can be employed.

### 6.2 Nesterov Method

We will provide a short summary of the application of Nesterov's multi-step method [Nes04] to the saddle point problem (86) as proposed in [LBS09]. In contrast to the FPD method, it treats the nonsmoothness by first applying a smoothing step and then using a smooth constrained optimization method. The amount of smoothing is balanced in such a way that the overall number of iterations to produce a solution with a specific accuracy is minimized.

The algorithm has a theoretical worst-case complexity of  $O(1/\varepsilon)$  for finding an  $\varepsilon$ -optimal solution, i.e.  $f(u^{(N)}) - f(u^*) \leq \varepsilon$ . It has been shown to

---

**Algorithm 3** Nesterov Multi-Class Labeling

---

- 1: Let  $c_1 \in \mathcal{C}$ ,  $c_2 \in \mathcal{D}$  and  $r_1, r_2 \in \mathbb{R}$  such that  $\mathcal{C} \subseteq \mathcal{B}_{r_1}(c_1)$  and  $\mathcal{D} \subseteq \mathcal{B}_{r_2}(c_2)$ ;  
 $C \geq \|L\|$ .
  - 2: Choose  $x^{(0)} \in \mathcal{C}$  and  $N \in \mathbb{N}$ .
  - 3: Let  $\mu \leftarrow \frac{2\|L\|}{N+1} \frac{r_1}{r_2}$ .
  - 4: Set  $G^{(-1)} \leftarrow 0, w^{(-1)} \leftarrow 0$ .
  - 5: **for**  $k = 0, \dots, N$  **do**
  - 6:    $V \leftarrow \Pi_{\mathcal{D}} \left( c_2 + \frac{1}{\mu} (Lx^{(k)} - b) \right)$ .
  - 7:    $w^{(k)} \leftarrow w^{(k-1)} + (k+1)V$ .
  - 8:    $v^{(k)} \leftarrow \frac{2}{(k+1)(k+2)} w^{(k)}$ .
  - 9:    $G \leftarrow s + L^\top V$ .
  - 10:    $G^{(k)} \leftarrow G^{(k-1)} + \frac{k+1}{2} G$ .
  - 11:    $u^{(k)} \leftarrow \Pi_{\mathcal{C}} \left( x^{(k)} - \frac{\mu}{\|L\|^2} G \right)$ .
  - 12:    $z^{(k)} \leftarrow \Pi_{\mathcal{C}} \left( c_1 - \frac{\mu}{\|L\|^2} G^{(k)} \right)$ .
  - 13:    $x^{(k+1)} \leftarrow \frac{2}{k+3} z^{(k)} + \left( 1 - \frac{2}{k+3} \right) u^{(k)}$ .
  - 14: **end for**
- 

give accurate results for denoising [Auj08] and general  $\ell_1$ -norm based problems [WABF07, BBC09]. Besides the desired accuracy, no other parameters have to be provided. The complete algorithm for our saddle point formulation is shown in Alg. 3.

The only expensive operations are the projections  $\Pi_{\mathcal{C}}$  and  $\Pi_{\mathcal{D}}$ , which are efficiently computable as shown above. The algorithm converges in any case and provides explicit suboptimality bounds:

**Proposition 8.** *In Alg. 3, the iterates  $u^{(k)}, v^{(k)}$  are primal resp. dual feasible, i.e.  $u^{(k)} \in \mathcal{C}$ ,  $v^{(k)} \in \mathcal{D}$ . Moreover, for any solution  $u^*$  of the relaxed problem (86), the relation*

$$f(u^{(N)}) - f(u^*) \leq f(u^{(N)}) - f_D(v^{(N)}) \leq \frac{2r_1r_2C}{(N+1)} \quad (108)$$

holds for the final iterates  $u^{(N)}, v^{(N)}$ .

*Proof.* Apply [Nes04, Thm. 3] with the notation  $\hat{f}(u) = \langle u, s \rangle$ ,  $A = L$ ,  $\hat{\phi}(v) = \langle b, v \rangle$ ,  $d_1(u) := \frac{1}{2}\|u - c_1\|^2$ ,  $d_2(v) := \frac{1}{2}\|v - c_2\|^2$ ,  $D_1 = \frac{1}{2}r_1^2$ ,  $D_2 = \frac{1}{2}r_2^2$ ,  $\sigma_1 = \sigma_2 = 1$ ,  $M = 0$ .  $\square$

**Corollary 1.** *For given  $\varepsilon > 0$ , applying Alg. 3 with*

$$N = \lceil 2r_1r_2C\varepsilon^{-1} - 1 \rceil \quad (109)$$

*yields an  $\varepsilon$ -optimal solution of (86), i.e.  $f(u^{(N)}) - f(u^*) \leq \varepsilon$ .*

For the discretization outlined in Sect. 5.2, we choose  $c_1 = \frac{1}{l}e$  and  $r_1 = \sqrt{n(l-1)/l}$ , which leads to the following complexity bounds to  $u^{(N)}$  with respect to the suboptimality  $\varepsilon$ .

- *Envelope method (95)*. From the previous remarks,  $C := 2\sqrt{d} \geq \|L\|$ . Moreover  $c_2 = 0$  and by Prop. 10 (see Appendix), we have  $\mathcal{D}_{\text{loc}}^d \subseteq \mathcal{B}_{\alpha_d}(0)$  with

$$\alpha_d := \min_i \left( \sum_j d(i, j)^2 \right)^{1/2}, \quad (110)$$

and thus  $r_2 = \alpha_d \sqrt{n}$ . The total complexity in terms of the number of iterations is

$$O(\varepsilon^{-1} n \sqrt{d} \alpha_d). \quad (111)$$

- *Euclidean metric method (96)*. Here we may set  $C = 2\sqrt{d}\|A\|$ ,  $c_2 = 0$  and  $r_2 = \sqrt{n}$  for a total complexity of

$$O(\varepsilon^{-1} n \sqrt{d} \|A\|). \quad (112)$$

We arrive at a parameter-free algorithm, with the exception of the desired sub-optimality bound. From the sequence  $(u^{(k)}, v^{(k)})$  we may again compute the current primal-dual gap at each iteration. As a unique feature, the number of required iterations can be determined a priori and independently of the variables in the data term, which could prove useful in real-time applications.

### 6.3 Douglas-Rachford Method

We demonstrate how to apply the Douglas-Rachford splitting approach [DR56] to our problem. By introducing auxiliary variables, we can again reduce the inner steps to projections on the sets  $\mathcal{C}$  and  $\mathcal{D}$ . This is in contrast to a more straightforward splitting approach such as [LKY<sup>+</sup>09], where the inner steps require to solve ROF-type problems that include a quadratic data term.

Minimizing a proper, convex, lower-semicontinuous (*lsc*) function  $f : X \rightarrow \mathbb{R} \cup \{\pm\infty\}$  over a finite dimensional vector space  $X := \mathbb{R}^n$  can be regarded as finding a zero of its – necessarily maximal monotone [RW04] – subdifferential operator  $T := \partial f : X \rightarrow 2^X$ . In the operator splitting framework,  $\partial f$  is assumed to be decomposable into the sum of two “simple” operators,  $T = A + B$ , of which forward and backward steps can practically be computed. Here, we consider the (tight) *Douglas-Rachford-Splitting* iteration [DR56, LM79] with the fixpoint iteration

$$\bar{u}^{(k+1)} = (J_{\tau A}(2J_{\tau B} - I) + (I - J_{\tau B}))(\bar{u}^{(k)}), \quad (113)$$

where  $J_{\tau T} := (I + \tau T)^{-1}$  is the *resolvent* of  $T$ . Under the very general constraint that  $A$  and  $B$  are maximal monotone and  $A + B$  has at least one zero, the sequence  $(\bar{u}^{(k)})$  is uniquely defined and will converge to a point  $\bar{u}$ , with the additional property that  $u := J_{\tau B}(\bar{u})$  is a zero of  $T$  [Eck89, Thm. 3.15, Prop. 3.20, Prop. 3.19]. In particular if  $f = f_1 + f_2$  for proper, convex, lsc  $f_i$  such that the relative interiors of their domains have a nonempty intersection,

$$\text{ri}(\text{dom } f_1) \cap \text{ri}(\text{dom } f_2) \neq \emptyset, \quad (114)$$

it follows [RW04, Cor. 10.9] that  $\partial f = \partial f_1 + \partial f_2$ , and  $A := \partial f_1$ ,  $B := \partial f_2$  are maximal monotone. As  $x \in J_{\tau \partial f_i}(y) \Leftrightarrow x = \arg \min\{(2\tau)^{-1}\|x-y\|_2^2 + f_i(x)\}$ , the computation of the resolvents reduces to proximal point optimization problems involving only the  $f_i$ . However, for straightforward splittings of (86), such as

$$\min_u \max_{v \in \mathcal{D}} \underbrace{g(u, v)}_{f_1(u)} + \underbrace{\delta_{\mathcal{C}}(u)}_{f_2(u)}, \quad (115)$$

evaluating the resolvents requires to solve ROF-type problems [LKY<sup>+</sup>09], which is a strongly non-local operation and requires an iterative procedure, introducing additional parameters and convergence issues. Instead, we follow the procedure in [EB92, Set09b] of adding auxiliary variables before splitting the objective in order to simplify the individual steps of the algorithm. We introduce  $w = Lu$  and split according to

$$\min_{u \in \mathcal{C}} \max_{v \in \mathcal{D}} \langle u, s \rangle + \langle Lu, v \rangle - \langle b, v \rangle \quad (116)$$

$$= \min_u \langle u, s \rangle + \sigma_{\mathcal{D}}(Lu - b) + \delta_{\mathcal{C}}(u) \quad (117)$$

$$= \min_{u, w} h(u, w) := \underbrace{\delta_{Lu=w}(u, w)}_{h_1(u, w)} + \underbrace{\langle u, s \rangle + \delta_{\mathcal{C}}(u) + \sigma_{\mathcal{D}}(w - b)}_{h_2(u, w)}. \quad (118)$$

We apply the tight Douglas-Rachford iteration to this formulation: Denote

$$(u^{(k)}, w^{(k)}) := J_{\tau \partial B}(\bar{u}^{(k)}, \bar{w}^{(k)}), \quad (119)$$

$$\begin{aligned} (u'^{(k)}, w'^{(k)}) &:= J_{\tau A}(2J_{\tau B} - I)(\bar{u}^{(k)}, \bar{w}^{(k)}) \\ &= J_{\tau A}(2u^{(k)} - \bar{u}^{(k)}, 2w^{(k)} - \bar{w}^{(k)}). \end{aligned} \quad (120)$$

Then  $(\bar{u}^{(k+1)}, \bar{w}^{(k+1)}) = (\bar{u}^{(k)} + u'^{(k)} - u^{(k)}, \bar{w}^{(k)} + w'^{(k)} - w^{(k)})$ , according to (113). Evaluating the resolvent  $J_{\tau B}$  is equivalent to a proximal step on  $h_2$ ; moreover due to the introduction of the auxiliary variables it decouples,

$$\begin{aligned} u'^{(k)} &= \arg \min_{u'} \left\{ \frac{1}{2} \|u' - (2u^{(k)} - \bar{u}^{(k)}) + \tau s\|_2^2 + \delta_{\mathcal{C}}(u') \right\} \\ &= \Pi_{\mathcal{C}} \left( (2u^{(k)} - \bar{u}^{(k)}) - \tau s \right), \end{aligned} \quad (121)$$

$$\begin{aligned} w'^{(k)} &= \arg \min_{w'} \left\{ \frac{1}{2\tau} \|w' - (2w^{(k)} - \bar{w}^{(k)})\|_2^2 + \sigma_{\mathcal{D}}(w' - b) \right\} \\ &= (2w^{(k)} - \bar{w}^{(k)}) - \tau \Pi_{\mathcal{D}} \left( \frac{1}{\tau} (2w^{(k)} - \bar{w}^{(k)} - b) \right). \end{aligned} \quad (122)$$

In a similar manner,  $J_{\tau A}$  resp. the proximal step on  $h_1$  amounts to the least-squares problem

$$(u^{(k)}, w^{(k)}) = \arg \min_{u, w} \left\{ \frac{1}{2\tau} \left( \|u - \bar{u}^{(k)}\|_2^2 + \|w - \bar{w}^{(k)}\|_2^2 \right) + \delta_{Lu=w}(u, w) \right\}. \quad (123)$$

Substituting the constraint  $w^{(k)} = Lu^{(k)}$  yields

$$\begin{aligned} u^{(k)} &= \arg \min_u \{ \|u - \bar{u}^{(k)}\|_2^2 + \|Lu - \bar{w}^{(k)}\|_2^2 \} \\ &= (I + L^\top L)^{-1} \left( \bar{u}^{(k)} + L^\top \bar{w}^{(k)} \right). \end{aligned} \quad (124)$$

---

**Algorithm 4** Douglas-Rachford Multi-Class Labeling

---

```

1: Choose  $\bar{u}^{(0)} \in \mathbb{R}^{n \times l}$ ,  $\bar{w}^{(0)} \in \mathbb{R}^{n \times d \times l}$  (or set  $\bar{w}^{(0)} = L\bar{u}^{(0)}$ ).
2: Choose  $\tau > 0$ .
3:  $k \leftarrow 0$ .
4: while (not converged) do
5:    $u^{(k)} \leftarrow \Pi_{\mathcal{C}} (\bar{u}^{(k)} - \tau s)$ .
6:    $w''^{(k)} \leftarrow \Pi_{\mathcal{D}} (\frac{1}{\tau}(\bar{w}^{(k)} - b))$ .
7:    $u'^{(k)} \leftarrow (I + L^\top L)^{-1} ((2u^{(k)} - \bar{u}^{(k)}) + L^\top (\bar{w}^{(k)} - 2\tau w''^{(k)}))$ .
8:    $w'^{(k)} \leftarrow Lu'^{(k)}$ .
9:    $\bar{u}^{(k+1)} \leftarrow \bar{u}^{(k)} + u'^{(k)} - u^{(k)}$ .
10:   $\bar{w}^{(k+1)} \leftarrow w'^{(k)} + \tau w''^{(k)}$ .
11:   $k \leftarrow k + 1$ .
12: end while

```

---

Finally, Alg. 4 is obtained by substituting  $w''^{(k)} := \Pi_{\mathcal{D}} (\frac{1}{\tau}(2w^{(k)} - \bar{w}^{(k)} - b))$ .

Solving the linear equation system (124) can often be greatly accelerated by exploiting the fact that under the forward difference discretization with Neumann boundary conditions,  $\text{grad}^\top \text{grad}$  diagonalizes under the discrete cosine transform (DCT-2) [Str99, LKY<sup>+</sup>09]:

$$\text{grad}^\top \text{grad} = B^{-1} \text{diag}(c)B \quad (125)$$

where  $B$  is the orthogonal transformation matrix of the DCT and  $c$  is the vector of eigenvalues of the discrete Laplacian. In both approaches presented above,  $L$  is of the form  $L = A \otimes \text{grad}$  for some (possibly identity) matrix  $A \in \mathbb{R}^{k \times l}$ ,  $k \leq l$ . First, compute the decomposition  $A^\top A = V^{-1} \text{diag}(a)V$  with  $a \in \mathbb{R}^l$  and an orthogonal matrix  $V \in \mathbb{R}^{l \times l}$ ,  $V^{-1} = V^\top$ . Then

$$\begin{aligned} (I + L^\top L)^{-1} &= (V^\top \otimes I_n) (I_l \otimes B^{-1}) \cdot \\ &\quad (I + \text{diag}(a) \otimes \text{diag}(c))^{-1} (I_l \otimes B) (V \otimes I_n) \end{aligned} \quad (126)$$

(see Appendix for the proof). Thus step 124 can be achieved fast and accurately through matrix multiplications with  $V$ , discrete cosine transforms, and one  $O(nl)$  product for inverting the inner diagonal matrix.

In addition to convergence of the primal iterates  $(u^{(k)})$ , it can be shown that the sequence  $(w''^{(k)})$  from Alg. 4 actually converges to a solution of the dual problem:

**Proposition 9.** *Let  $\mathcal{C}$ ,  $\mathcal{D}$  be bounded, closed and convex sets with  $\text{ri}(\mathcal{C}) \neq \emptyset$  and  $\text{ri}(\mathcal{D}) \neq \emptyset$ . Then Alg. 4 generates a sequence of primal/dual feasible pairs  $(u^{(k)}, w''^{(k)}) \in \mathcal{C} \times \mathcal{D}$  such that, for any saddle point  $(u^*, v^*)$  of the relaxed problem (86),*

$$f(u^{(k)}) \xrightarrow[k \rightarrow \infty]{} f(u^*) = f_D(v^*), \quad (127)$$

$$f_D(w''^{(k)}) \xrightarrow[k \rightarrow \infty]{} f_D(v^*) = f(u^*). \quad (128)$$

Moreover,

$$f(u^{(k)}) - f(u^*) \leq f(u^{(k)}) - f_D(w''^{(k)}) \quad (129)$$

provides an upper bound for the suboptimality of the current iterate.

*Proof.* See Appendix.  $\square$

Thus the Douglas-Rachford approach also allows to use the primal-dual gap

$$f(u^{(k)}) - f_D(w''^{(k)}) \quad (130)$$

as a stopping criterion.

Very recently, a generalization of the FPD method [PCBC09a] has been proposed [CP10]. The authors show that under certain circumstances, their method is equivalent to Douglas-Rachford splitting. As a result, it is possible to show that Alg. 4 can alternatively be interpreted as an application of the primal-dual method from [CP10] to the problem formulation (118).

## 6.4 Projection on the Dual Constraint Set

For the Euclidean metric approach, projection on the unit ball  $\mathcal{D}_{\text{loc}}^I$  and thus on  $\mathcal{D}$  is trivial:

$$\Pi_{\mathcal{D}_{\text{loc}}^I}(v) = \begin{cases} v, & \|v\| \leq 1, \\ \frac{v}{\|v\|}, & \text{otherwise.} \end{cases} \quad (131)$$

Projection on  $\mathcal{D}_{\text{loc}}^d$  for the general metric case is more involved. We represent  $\mathcal{D}_{\text{loc}}^d$  as the intersection of convex sets,

$$\begin{aligned} \mathcal{D}_{\text{loc}}^d &= \mathcal{R} \cap \mathcal{S}, \quad \mathcal{R} := \{v \in \mathbb{R}^{d \times l} \mid \sum_i v^i = 0\}, \\ \mathcal{S} &:= \bigcap_{i < j} \mathcal{S}^{i,j}, \quad \mathcal{S}^{i,j} := \{v \in \mathbb{R}^{d \times l} \mid \|v^i - v^j\| \leq d(i, j)\}. \end{aligned} \quad (132)$$

Since  $\Pi_{\mathcal{R}}$  amounts to a translation along  $e = (1, \dots, 1)$ , and  $\mathcal{S}$  is translation invariant in the direction of  $e$ , the projection can be decomposed:

$$\Pi_{\mathcal{D}_{\text{loc}}^d}(v) = \Pi_{\mathcal{R}}(\Pi_{\mathcal{S}}(v)). \quad (133)$$

We then follow the idea of [CCP08] to use Dykstra's method [BD86] for iteratively computing an approximation of  $\Pi_{\mathcal{S}}$  using only projections on the individual sets  $\mathcal{S}^{i,j}$ . However, any recent multiple-splitting method could be used [CP08, GM09]. In our case,  $\Pi_{\mathcal{S}^{i,j}}$  can be stated in closed form:

$$\Pi_{\mathcal{S}^{i,j}}(v) = \begin{cases} v, & \|v^i - v^j\| \leq d(i, j), \\ (w^1, \dots, w^l), & \text{otherwise,} \end{cases} \quad (134)$$

where

$$w^k = \begin{cases} v^k, & k \notin \{i, j\}, \\ v^i - \frac{\|v^i - v^j\| - d(i, j)}{2} \frac{v^i - v^j}{\|v^i - v^j\|}, & k = i, \\ v^j + \frac{\|v^i - v^j\| - d(i, j)}{2} \frac{v^i - v^j}{\|v^i - v^j\|}, & k = j. \end{cases} \quad (135)$$

The complete Dykstra method for projecting a vector  $v$  onto  $\mathcal{S}$  is outlined in Alg. 5. While the sequence of  $y$  may be unbounded,  $x$  converges to  $\Pi_{\mathcal{S}}(v)$  (cf. [GM89, Xu00]).



---

**Algorithm 5** Dykstra’s Method for Projecting onto the Intersection of Convex Sets

---

```

1: Associate with each  $(i, j), i < j$  a unique index  $t \in \{1, \dots, k\}$ ,  $k := l(l-1)$ .
2:  $x \leftarrow v \in \mathbb{R}^{d \times l}$ .
3:  $y^1, \dots, y^k \leftarrow 0 \in \mathbb{R}^{d \times l}$ .
4: while ( $x$  not converged) do
5:   for  $t = 1, \dots, k$  do
6:      $x' \leftarrow \Pi_{S^{(i_t, j_t)}}(x + y^t)$ .
7:      $y^t \leftarrow x + y^t - x'$ .
8:      $x \leftarrow x'$ .
9:   end for
10: end while

```

---

## 6.5 Computing the Objective

For computing the primal-dual gap and the binarization step, it is necessary to evaluate the objective for a given  $u$ . Unfortunately, in the general case this is nontrivial as the objective’s integrand  $\Psi$  is defined implicitly as

$$\Psi(z) = \max_{v \in \mathcal{D}_{\text{loc}}^d} \langle z, v \rangle. \quad (136)$$

We exploit that  $\Pi_{\mathcal{D}}$  can be computed and use an iterative gradient-projection method,

$$v^{(k+1)} \leftarrow \Pi_{\mathcal{D}}(v^{(k)} + \tau z) \quad (137)$$

for some  $\tau > 0$ , starting with  $v^{(0)} = z$ . As the objective in (136) is linear,  $\mathcal{D}_{\text{loc}}^d$  is bounded and thus  $\Psi$  is bounded from above, convergence follows [Gol64, LP66] for any step size  $\tau$  [WX04]:

$$\lim_{k \rightarrow \infty} \langle z, v^{(k)} \rangle = \Psi(z). \quad (138)$$

There is a trade-off in choosing the step size, as large  $\tau$  lead to a smaller number of outer iterations, but an increased number of nontrivial operations in the projection. We chose  $\tau = 2$ , which worked well for all examples. It is also possible to use any of the other nonsmooth optimization methods presented above.

## 7 Experiments

Regarding the practical performance of the presented approaches, we focused on two main issues: convergence speed and tightness of the relaxation. We will first quantitatively compare the presented algorithms in terms of runtime and the number of inner iterations, and then provide some results on the effect of the Euclidean metric vs. the envelope regularization.

The algorithms were implemented in Matlab with some core functions, such as the computation of the gradient and the projections on the dual sets, implemented in C++. We used Matlab’s built-in FFTW interface for computing the DCT for the Douglas-Rachford approach. All experiments were conducted on an Intel Core2 Duo 2.66 GHz with 4 GB of RAM and 64-bit Matlab 2009a.

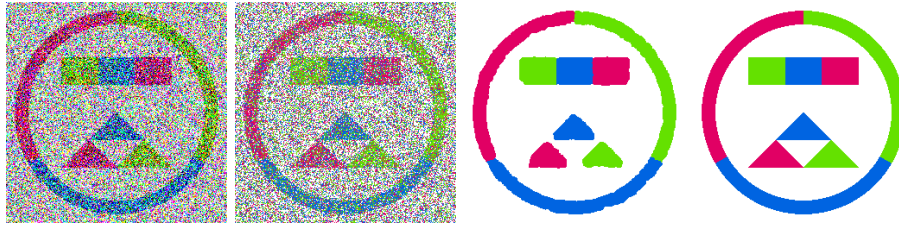


Figure 8: Synthetic “four colors” input image for the performance tests. **Top row:** Input image with Gaussian noise,  $\sigma = 1$ ; local labeling without regularizer. **Bottom row:** Result with the Potts regularizer and Douglas-Rachford optimization; ground truth.

## 7.1 Relative Performance

To compare the convergence speed of the three different approaches, we computed the relative primal-dual gap at each iteration as outlined in Sect. 6. As it bounds the suboptimality of the current iterate (see Sect. 5.5), it constitutes a reliable and convenient criterion for performance comparison.

Unfortunately the gap is not available for the envelope method, as it requires the primal objective to be evaluable. Using a numerical approximation such as the one in Sect. 6.5 is not an option, as these methods can only provide a *lower* bound for the objective. This would lead to an underestimation of the gap, which is critical as one is interested in the behavior when the gap is very close to zero. Therefore we restricted the gap-based performance tests to the Euclidean metric regularizer.

In order to make a fair comparison we generally analyzed the progression of the gap with respect to computation time, rather than the number of iterations.

For the first tests we used the synthetic  $256 \times 256$  “four colors” input image (Fig. 8). It represents a typical segmentation problem with several objects featuring sharp corners and round structures above a uniform background. The label set consists of three classes for the foreground and one class for the background. The image was overlaid with iid Gaussian noise with  $\sigma = 1$  and truncated to  $[0, 1]$  on all RGB channels. We used a simple  $\ell^1$  data term,  $s_i(x) = \|g(x) - c^i\|_1$ , where  $g(x) \in [0, 1]^3$  are the RGB color values of the input image in  $x$ , and  $c^i$  is a prototypical color vector for the  $i$ -th class.

The runtime analysis shows that FPD and Douglas-Rachford perform similar, while the Nesterov method falls behind considerably in both the primal and the dual objective (Fig. 9).

The picture changes when considering the gap with respect to the number of iterations rather than time, eliminating influences of the implementation and system architecture. To achieve the same accuracy, Douglas-Rachford requires only one third of the iterations compared to FPD (Fig. 10). This advantage does not fully translate to the time-based analysis as the DCT steps increase the per-step computational cost significantly. However in this example the projections on the sets  $\mathcal{C}$  and  $\mathcal{D}$  were relatively cheap compared to the DCT. In situations where the projections dominate the time per step, the reduced iteration count can be expected to lead to an almost equal reduction in computation time.

One could ask if these relations are typical to the synthetic data used.

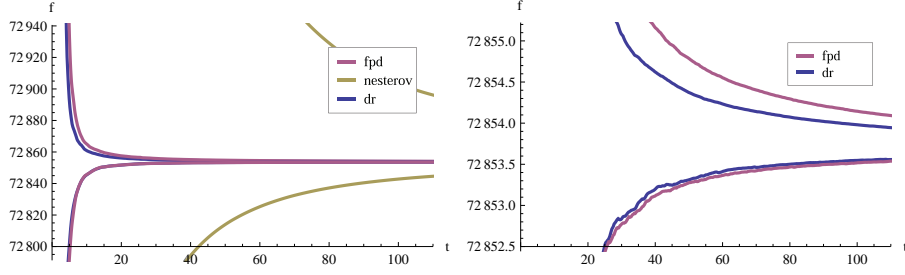


Figure 9: Convergence speed for the “four colors” image in Fig. 8. **Left:** Primal (upper) and dual (lower) objectives vs. computation time for the (from top to bottom) Nesterov, Fast Primal-Dual (FPD) and Douglas-Rachford methods. **Right:** Detailed view of the FPD and DR methods. The primal and dual objectives provide upper and lower bounds for the objective of the true optimum. Douglas-Rachford and FPD perform equally, while the Nesterov method falls behind.

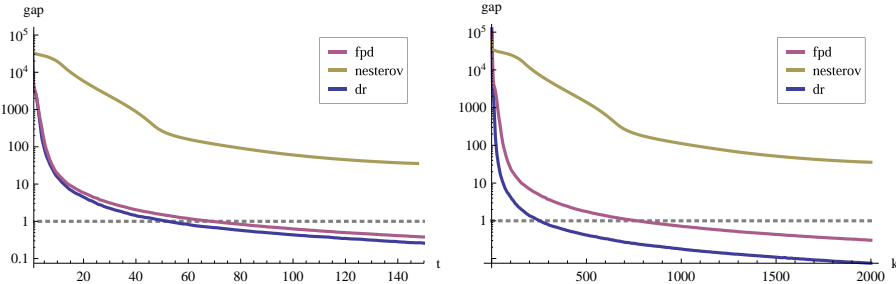


Figure 10: Primal-Dual gap for Fig. 9 with respect to time and number of iterations. **Top:** Primal-Dual gap vs. time and number of iterations. The Nesterov method (top) again falls behind, while FPD (center) and Douglas-Rachford (bottom) are equally fast. **Bottom:** Primal-Dual gap vs. number of iterations. The Douglas-Rachford method requires only one third of the FPD iterations, which makes it suitable for problems with expensive inner steps.

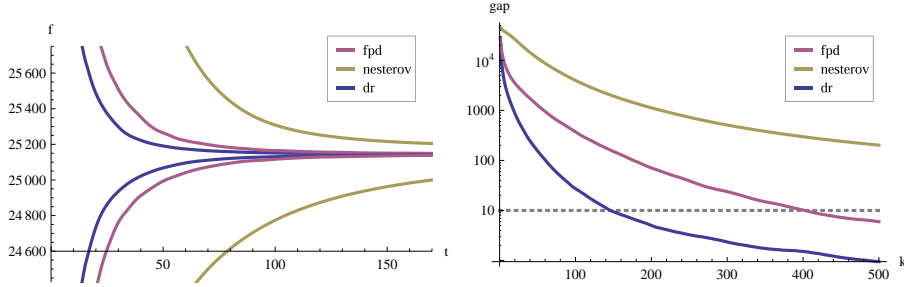


Figure 11: Objectives and primal-dual gap for the real-world leaf image in Fig. 4 with 12 classes and Potts potential. **Left:** Primal (upper) and dual (lower) objectives vs. time. The Nesterov method (top) falls behind the FPD (center) and Douglas-Rachford (bottom) methods. **Right:** Gap vs. number of iterations. As with the synthetical four-colors image (Fig. 10), the Douglas-Rachford approach reduces the number of required iterations by approximately a factor of 3.

However we found them confirmed on a large majority of the problems tested. As one example of a real-world example, consider the “leaf” image (Fig. 4). We computed a segmentation into 12 classes with Potts regularizer, again based on the  $\ell^1$  distances for the data term, with very similar relative performance as for the “four colors” image (Fig. 11).

## 7.2 Number of Variables and Regularization Strength

To examine how the presented methods scale with increasing image size, we evaluated the “four colors” image at 20 different scales ranging from  $16 \times 16$  to  $512 \times 512$ . Note that if the grid spacing is held constant, the regularizer weights must be scaled proportionally to the image width resp. height in order to obtain structurally comparable results, and not mix up effects of the problem size and of the regularization strength.

In order to compensate for the increasing number of variables, the stopping criterion was based on the relative gap (101). The algorithms terminated as soon as the relative gap fell below  $10^{-4}$ . The Nesterov method consistently produced gaps in the  $10^{-3}$  range and never achieved the threshold within the limit of 2000 iterations. Douglas-Rachford and FPD scale only slightly superlinearly with the problem size, which is quite a good result for such comparatively simple first-order methods (Fig. 12).

While we deliberately excluded influences of the regularizer in the previous experiment, it is also interesting to examine how algorithms cope with varying regularization strength. We fixed a resolution of  $256 \times 256$  and performed the same analysis as above, scaling the regularization term by an increasing sequence of  $\lambda$  in the  $[0.1, 5]$  range (Fig. 13).

Interestingly, for low regularization, where much of the noise remains in the solution, FPD clearly takes the lead. For scenarios with large structural changes, Douglas-Rachford performs better. We observed two peaks in the runtime plot which we cannot completely explain. However we found that at the first peak, structures in the image did not disappear at in parallel but rather one after the

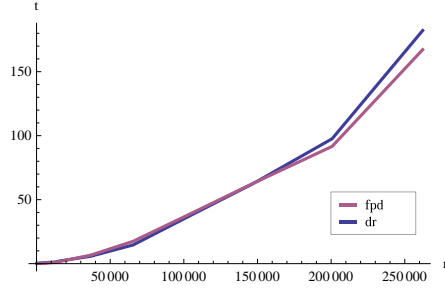


Figure 12: Computation time for increasing problem size for the Douglas-Rachford (top, dark) and FPD (bottom, light) methods. Shown is the time in seconds required to achieve a relative gap of  $10^{-4}$ . The computational effort scales slightly superlinearly with the number of pixels. The Nesterov method never converged to the required accuracy within the limit of 2000 iterations.

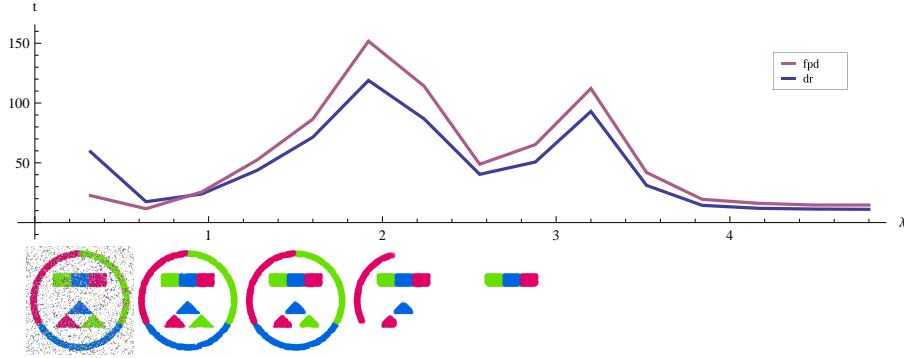


Figure 13: Computation time for varying regularization strength  $\lambda$  for the Douglas-Rachford (top, dark) and FPG (bottom, light) methods. The images at the bottom show the final result for the  $\lambda$  above. FPD is strong on low regularization problems, while Douglas-Rachford is better suited for problems with large structural changes. The Nesterov method never achieved the relative gap of  $10^{-5}$  within 2000 iterations.

other, which might contribute to the slower convergence. Again, the Nesterov method never achieved the required accuracy.

### 7.3 Breaking Points

We have no clear explanation why the Nesterov method appears to almost always fall behind. However it is possible to compare its behavior with the a priori bound from Prop. 8. By inspecting the derivations in the original work [Nes04], it can be seen that exactly one half of the final bound comes from the smoothing step, while the other half is caused by the finite number of iterations:

$$\delta_{\text{total}} = \delta_{\text{smooth}} + \delta_{\text{iter}}, \quad \text{where} \quad \delta_{\text{smooth}} = \delta_{\text{iter}}. \quad (139)$$

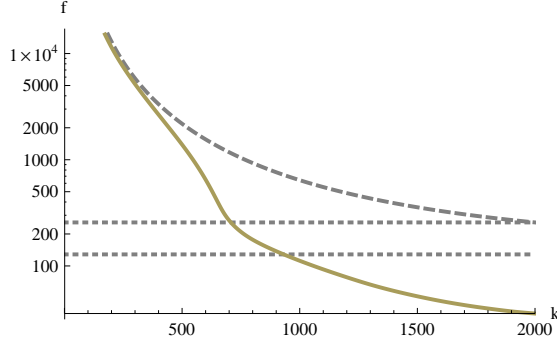


Figure 14: Theoretical vs. practical performance of the Nesterov method for Fig. 9. As expected, the method stays below the theoretical per-iteration bound  $\delta_{\text{total}}^{(k)}$  (dashed). At the final iteration, the worst-case total bound  $\delta_{\text{total}}$  (dotted, top) is outperformed by a factor of 7, which implicates that the error introduced by smoothing is also well below its worst-case bound  $\delta_{\text{smooth}}$  (dotted, bottom).

Moreover,  $\delta_{\text{iter}}$  decreases with  $1/(k+1)^2$ , which gives an a priori per-iteration suboptimality bound of

$$\delta_{\text{total}}^{(k)} = \delta_{\text{smooth}} + \left( \frac{N+1}{k+1} \right)^2 \delta_{\text{iter}}. \quad (140)$$

On the “four colors” image, the actual gap stays just below  $\delta_{\text{total}}^{(k)}$  in the beginning (Fig. 14). This implies that the theoretical suboptimality bound can hardly be improved, e.g. by choosing constants more precisely. Unfortunately, the bound is generally rather large, in this case at  $\delta_{\text{total}} = 256.8476$  for 2000 iterations. While the Nesterov method outperforms the theoretical bound  $\delta_{\text{total}}$  by a factor of 2 to 10 and even drops well below the worst-case smoothing error  $\delta_{\text{smooth}}$ , it still cannot compete with the other methods, which achieve a gap of 0.3052 (FPD) resp. 0.0754 (Douglas-Rachford).

There is an interesting extreme case where the Nesterov method seems to come to full strength. Consider the noise-free “triple point” inpainting problem (Fig. 15). The triple junction in the center can only be reconstructed by the Potts regularizer, as the  $\ell^1$  data term has been blanked out around the center. By reversing the sign of the data term, one obtains the “inverse triple point” problem, an extreme case that has also been studied in [CCP08] and shown to be an example where the relaxation leads to a strictly nonbinary solution.

On the inverse problem, the Nesterov method catches up and even surpasses FPD. This stands in contrast with the regular triple point problem, where all methods perform as usual. We conjecture that this sudden strength comes from the inherent averaging over all previous gradients (step 7 in Alg. 3): in fact, on the inverse problem Douglas-Rachford and FPD display a pronounced oscillation in the primal and dual objectives, which is accompanied by slow convergence. In contrast, the Nesterov method consistently shows a monotone and smooth convergence.

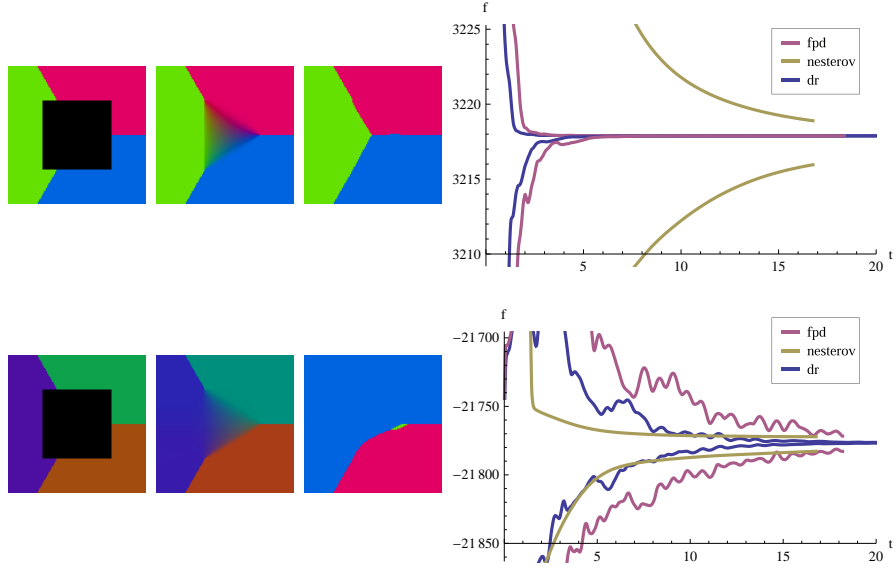


Figure 15: Primal and dual objectives for the triple point (top) and inverse triple point (bottom) inpainting problems. **Left to right:** Input image with zeroed-out region around the center; relaxed solution; binarized solution; primal (upper) and dual (lower) energies vs. time. The triple junction in the center has to be reconstructed solely by the Potts regularizer. The inverse triple point problem exhibits a strictly nonbinary relaxed solution. For the inverse triple point, Douglas-Rachford (bottom) and FPD (center) show an oscillatory behavior which slows down convergence. The Nesterov approach (top) does not suffer from oscillation due to the inherent averaging, and surpasses FPD on the inverse problem.

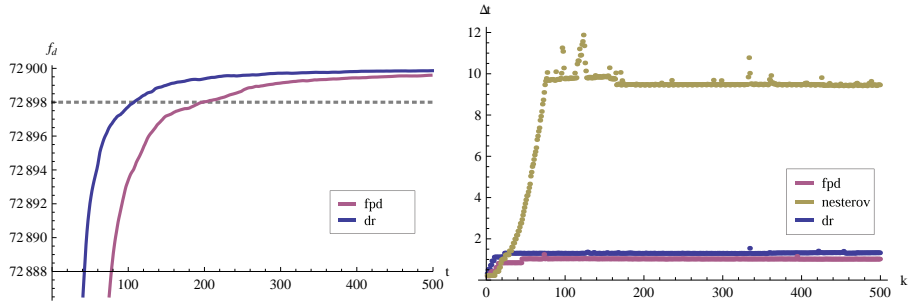


Figure 16: Performance on the “four colors” image with Potts interaction potential and the envelope regularizer. **Left:** Dual objectives of for Douglas-Rachford (top) and FPD (bottom) vs. time. The reduced iteration count of the Douglas-Rachford method becomes more apparent in the time plot as the time per iteration is now dominated by the projection rather than the DCT. **Right:** Time per iteration for Nesterov (top), Douglas-Rachford (center) and FPD (bottom). The Nesterov method fails to converge as it accumulates errors from the approximate projections, which in turn leads to slower and more inexact projections.

## 7.4 Performance for the Envelope Relaxation

Undoubtedly, the difficulty when using the envelope based regularizer comes from the slow and inexact projection steps which have to be approximated iteratively. Therefore we re-evaluated the “four colors” benchmark image with the envelope regularizer. The iterative Dykstra projection (Alg. 5) was stopped when the iterates differed by at most  $\delta = 10^{-2}$ , with an additional limit of 50 iterations. While the gap cannot be computed in this case, the dual objective can still be evaluated and provides an indicator for the convergence speed.

We found that in comparison to the Euclidean metric regularizer from the previous examples, the margin between FPD and Douglas-Rachford increases significantly. This is consistent with the remarks in Sect. 7.1: the lower iteration count of the Douglas-Rachford method becomes more important, as the projections dominate the per-iteration runtime (Fig. 16).

Surprisingly the Nesterov method did not converge at all. On inspecting the per-iteration runtime, we found that after the first few outer iterations, the iterative projections became very slow and eventually exceeded the limit of 50 iterations with  $\delta$  remaining between 2 and 5. In contrast, 20 Dykstra iterations were usually sufficient to obtain  $\delta = 10^{-9}$  (Douglas-Rachford) resp.  $\delta = 10^{-11}$  (FPD).

We again attribute this to the averaging property of the Nesterov method: as it accumulates the results of the previous projections, errors from the inexact projections build up. This is accelerated by the dual variables quickly becoming infeasible with increasing distance to the dual feasible set, which in turn puts higher demands on the iterative projections. Douglas-Rachford and FPD did not display this behavior and consistently required 5 to 6 Dykstra iterations from the first to the last iteration.

## 7.5 Tightness of the Relaxations

Besides the properties of the optimization methods, it is interesting to study the effect of the relaxation – i.e. Euclidean metric or envelope type – on the relaxed and binarized solutions.

To get an insight into the tightness of the relaxations, we used the Douglas-Rachford method to repeat the “triple point” inpainting experiment in [CCP08] with both relaxations (Fig. 17). Despite the inaccuracies in the projections, the envelope regularizer generates a nearly binary solution: 97.6% of all pixels were assigned “almost binary” labels with an  $\ell^\infty$  distance of less than 0.05 to one of the unit vectors  $\{e^1, \dots, e^l\}$ . For the Euclidean metric method, this constraint was only satisfied at 88.6% of the pixels. The result for the envelope relaxation is very close to the sharp triple junction one would expect from the continuous formulation, and shows that the envelope relaxation is tighter than the Euclidean metric method.

However, after binarization both approaches generate almost identical discrete results. The Euclidean metric method was more than four times faster, with 41.1 seconds per 1000 iterations vs. 172.16 seconds for the envelope relaxation, which required 8–11 Dykstra steps per outer iteration.

While the triple point is a problem specifically designed to challenge the regularizer, real-world images usually contain more structure as well as noise, while the data term is available for most or all of the image. To see if the above



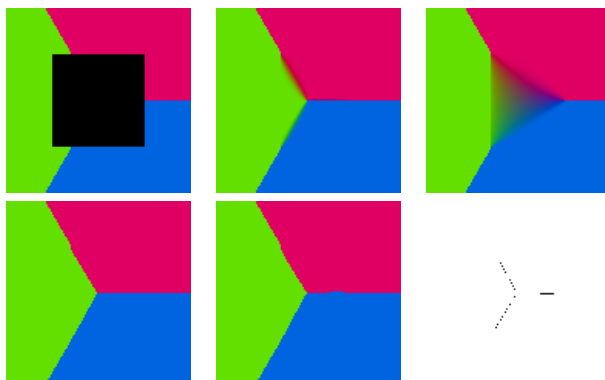


Figure 17: Tightness of the relaxation. **Top row:** In the input (left), the data term was blanked out in a quadratic region. All structure within the region is generated purely by the regularizer with a standard Potts interface potential. The envelope relaxation is tighter and generates a much more “binary” solution (center) than the Euclidean metric method (right). **Bottom row:** After binarization of the relaxed solutions, the envelope (left) and Euclidean metric (center) methods generate essentially the same solution, as can be seen in the difference image (right). The Euclidean metric method performed more than four times faster due to the inexpensive projections.

results also hold under these conditions, we repeated the previous experiment with the “sailing” image and four classes (Fig. 18). The improved tightness of the envelope relaxation was also noticeable, with 96.2% vs. 90.6% of “almost binary” pixels. However, due to the larger number of labels and the larger image size of  $360 \times 240$ , runtimes increased to 4253 (envelope) vs. 420 (Euclidean metric) seconds.

The relaxed as well as the binarized solutions show some differences but are hard to distinguish visually. It is difficult to pinpoint if these differences are caused by the tighter relaxation or by numerical issues: while the Douglas-Rachford method applied to the Euclidean metric relaxation converged to a final relative gap of  $1.5 \cdot 10^{-6}$ , no such bound is available to estimate the accuracy of the solution for the envelope relaxation, due to the inexact projections and the intractable primal objective.

## 7.6 Binarization and Global Optimality

As an example for a problem with a large number of classes, we analyzed the “penguin” inpainting problem from [SZS<sup>+</sup>06]. We chose 64 labels corresponding to 64 equally spaced gray values. The input image contains a region where the image must be inpainted in addition to removing the considerable noise. Again the data term was generated by the  $\ell^1$  distance, which reduces here to the absolute difference of the gray values. In order to remove noise but not overly penalize hard contrasts, such as between the black wing and the white front, we chose a regularizer based on the truncated linear potential as introduced in Sect. 4.4.

Due to the large number of labels, this problem constitutes an example

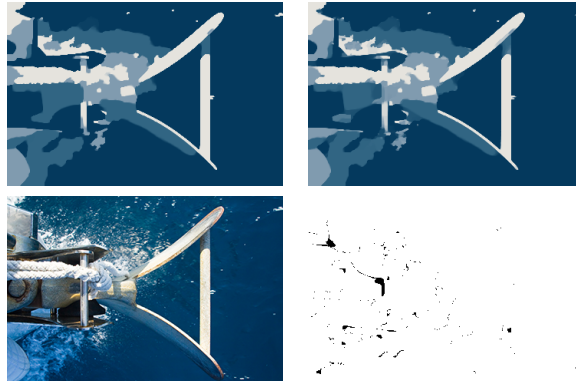


Figure 18: Effect of the choice of relaxation method on the real-world “sailing” image (image courtesy of F. Becker). **Top row:** Four-class segmentation using envelope (left) and Euclidean metric (right) methods. Shown are the solutions of the relaxed problem. **Bottom row:** Original image (left); difference image of the discretized solutions (right). While the envelope relaxation leads to substantially more “almost discrete” values in the relaxed solution, it also runs more than 10 times slower and does not provide a suboptimality bound. The generated solutions are visually almost identical.

where the Euclidean metric approach is very useful. As the complexity of the projections for the envelope relaxation grows quadratically with the number of labels, computation time becomes prohibitively long for a moderate amount of classes. In contrast, the Euclidean metric method requires considerably less computational effort and still approximate the potential function to a reasonable accuracy (Fig. 7).

In the practical evaluation, the Douglas-Rachford method converged in 1000 iterations to a relative gap of  $8.3 \cdot 10^{-4}$ , and recovered both smooth details near the beak, and hard edges in the inpainting region (Fig. 19). This example also clearly demonstrates the superiority of the improved binarization scheme proposed in Sect. 5.6. As opposed to the first-max scheme, the improved scheme generated considerably less noise. The energy increased only by 2.78% compared to 15.78% for the first-max approach.

The low energy increase is directly related to global optimality for the discrete problem: as the relaxed solution is provably nearly optimal, we conclude that the energy of the *binarized* solution must lie within 2.78% of the optimal energy for the original *combinatorial* problem (1). Similar results were obtained for the other images: 5.64% for the “four colors” demo, 1.02% for the “leaf” image and 0.98% for the “triple point” problem.

These numbers indicate that the relaxation seems to be quite tight in many cases, and allows to recover good approximations for the solution of the discrete combinatorial labeling problem by solving the convex relaxed problem.

## 8 Conclusion and Further Work

The present work provides a reference and framework for continuous multilabeling approaches. The presented algorithms are robust and fast and are suited for

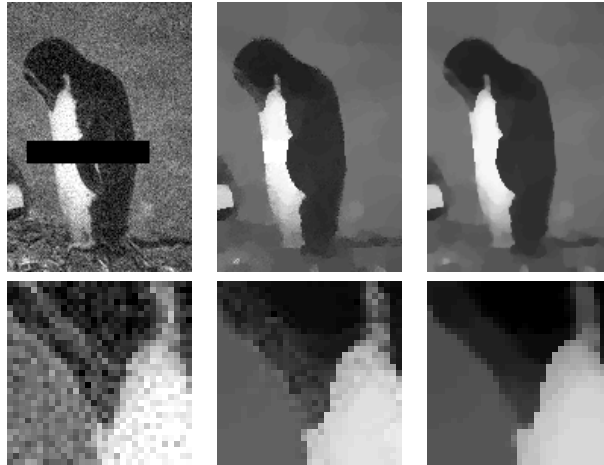


Figure 19: Denoising/inpainting problem with 64 classes and the nontrivial truncated linear potential approximated by an Euclidean metric. **Left to right:** Noisy input image with inpainting region marked black [SZS<sup>+</sup>06]; result with first-max binarization; result with the proposed binarization scheme (104). The first-max method introduces noticeable noise in the binarization step. The proposed method takes into account the non-uniformity of the used “cut-linear” potential (Fig. 7), resulting in a clean labeling and an energy increase of only 2.78% vs. 15.78% for the first-max method. This shows that the obtained solution solves the originally combinatorial multiclass labeling problem to a suboptimality of 2.78%.

massive parallelization. From the experiments it became clear that solving the convex relaxed problem allows to recover very good solutions for the original combinatorial problem in most cases.

The performance evaluations showed that the Douglas-Rachford method consistently requires about one third of the iterations compared to the Fast Primal-Dual method. For low regularization and fast projections, FPD outperforms the Douglas-Rachford method. In all other cases, Douglas-Rachford performs equally or better, with a speedup of 2-3 if the projections are expensive. Overall, the proposed Douglas-Rachford method approach appears to be a solid all-round method that also handles extreme cases well.

From the viewpoint of numerics, in our evaluations we did not specifically consider the effect of choosing different step sizes for the Douglas-Rachford method. Also, it seems as if the smooth optimization step in the Nesterov method usually performs much better than its theoretical bound. Adjusting the strategy for choosing the smoothing parameter could yield a faster overall convergence and possibly render the method competitive. In this regard, it would also be interesting to include the inexactness of the projections into the convergence analysis. There are also several theoretical questions left, such as how to include non-metric distances into the continuous formulation.

In any case we think that the present framework unites continuous and discrete worlds in an appealing way, and hopefully contributes to reducing the popularity gap compared to purely grid-based, graph cut methods.

**Acknowledgments.** The authors would like to thank Simon Setzer for the stimulating discussion. We are also grateful to an anonymous reviewer, whose extensive comments greatly helped to improve the presentation of this work.

## 9 Appendix

**Proposition 10.** Let  $v = (v^1, \dots, v^l) \in \mathcal{D}_{\text{loc}}^d$ , then

$$\|v\| \leq \min_i \left( \sum_j d(i, j)^2 \right)^{\frac{1}{2}}. \quad (141)$$

*Proof of Prop. 10.* From the constraint  $\sum_{j=1}^l v^j = 0$  in (70) we deduce, for arbitrary but fixed  $i \in \{1, \dots, l\}$ ,

$$\begin{aligned} \sum_{j=1}^l \|v^j\|^2 &\leq \left( \sum_{j=1}^l \|v^j\|^2 \right) - 0 + l\|v^i\|^2 \\ &= \left( \sum_{j=1}^l \|v^j\|^2 \right) - 2\langle v^i, \sum_{j=1}^l v^j \rangle + l\|v^i\|^2 \\ &= \sum_{j=1}^l (\|v^j\|^2 - 2\langle v^i, v^j \rangle + \|v^i\|^2) \\ &= \sum_{j=1}^l \|v^j - v^i\|^2 \leq \sum_{j=1}^l d(i, j)^2. \end{aligned} \quad (142)$$

As  $i$  was arbitrary this proves the assertion.  $\square$

*Proof of Eq. (126).* We mainly use the fact that  $(P \otimes Q)(R \otimes S) = (PR) \otimes (QS)$  for matrices  $P, Q, R, S$  with compatible dimensions:

$$(I + L^\top L)^{-1} = \left( I + (A \otimes \text{grad})^\top (A \otimes \text{grad}) \right)^{-1} \quad (143)$$

$$= \left( I + (A^\top A) \otimes (\text{grad}^\top \text{grad}) \right)^{-1} \quad (144)$$

$$= \left( I + (V^{-1} \text{diag}(a)V) \otimes (B^{-1} \text{diag}(c)B) \right)^{-1} \quad (145)$$

$$= \left( I + (V^{-1} \otimes B^{-1}) (\text{diag}(a) \otimes \text{diag}(c)) (V \otimes B) \right)^{-1} \quad (146)$$

$$= \left( (V^{-1} \otimes B^{-1}) (I + \text{diag}(a) \otimes \text{diag}(c)) (V \otimes B) \right)^{-1} \quad (147)$$

$$= (V^{-1} \otimes B^{-1}) (I + \text{diag}(a) \otimes \text{diag}(c))^{-1} (V \otimes B). \quad (148)$$

Using  $V^{-1} = V^\top$ , (126) follows.  $\square$

*Proof of Prop. 9.* The idea of the proof is to show that the sequence  $(w''^{(k)})$  is exactly the minimizing sequence produced by the algorithm applied to the dual problem (87), with step size  $1/\tau$ . Thus, if the dual algorithm converges,  $(w''^{(k)})$  converges to the solution of the dual problem, which proves the assertion. To

---

**Algorithm 6** Dual Douglas-Rachford for Multi-Class Labeling
 

---

```

1: Choose  $\bar{v}^{(0)} \in \mathbb{R}^{n \times d \times l}$ ,  $\bar{z}^{(0)} \in \mathbb{R}^{n \times l}$ .
2: Choose  $\tau_D > 0$ .
3:  $k \leftarrow 0$ .
4: while (not converged) do
5:    $v^{(k)} \leftarrow \Pi_{\mathcal{D}} (\bar{v}^{(k)} - \tau_D b)$ .
6:    $z''^{(k)} \leftarrow \Pi_{\mathcal{C}} \left( \frac{1}{\tau_D} (\bar{z}^{(k)} - s) \right)$ .
7:    $v'^{(k)} \leftarrow (I + LL^\top)^{-1} ((2v^{(k)} - \bar{v}^{(k)}) + (-L)(\bar{z}^{(k)} - 2\tau_D z''^{(k)}))$ .
8:    $z'^{(k)} \leftarrow (-L^\top)v'^{(k)}$ .
9:    $\bar{v}^{(k+1)} \leftarrow \bar{v}^{(k)} + v'^{(k)} - v^{(k)}$ .
10:   $\bar{z}^{(k+1)} \leftarrow \bar{z}^{(k)} + \tau_D z''^{(k)}$ .
11:   $k \leftarrow k + 1$ .
12: end while

```

---

show the equivalency, first note that the formulation of the primal problem from (86),

$$\min_{u \in \mathcal{C}} \max_{v \in \mathcal{D}} \langle u, s \rangle + \langle Lu, v \rangle - \langle b, v \rangle \quad (149)$$

already covers the dual problem

$$\begin{aligned} & \max_{v \in \mathcal{D}} \min_{u \in \mathcal{C}} \langle u, s \rangle + \langle Lu, v \rangle - \langle b, v \rangle \\ &= \min_{v \in \mathcal{D}} \max_{u \in \mathcal{C}} \langle b, v \rangle + \langle u, -L^\top v \rangle - \langle u, s \rangle \end{aligned} \quad (150)$$

by the substitutions

$$v \leftrightarrow u, \mathcal{C} \leftrightarrow \mathcal{D}, b \leftrightarrow s, L \leftrightarrow -L^\top. \quad (151)$$

The dual problem can thus be solved by applying the above substitutions to Alg. 4. Additionally substituting  $w \leftrightarrow z$  in Alg. 4 in order to avoid confusion with iterates of the primal method, leads to the dual algorithm, Alg. 6. We first show convergence of Alg. 4 and Alg. 6. By construction, these amount to applying Douglas-Rachford splitting to the primal resp. dual formulations

$$\min_{u, w} \underbrace{\delta_{Lu=w}(u, w)}_{=: h_1(u, w)} + \underbrace{\langle u, s \rangle + \delta_{\mathcal{C}}(u) + \sigma_{\mathcal{D}}(w - b)}_{=: h_2(u, w)}, \quad (152)$$

$$\min_{v, z} \underbrace{\delta_{-L^\top v=z}(v, z)}_{=: h_{D,1}(v, z)} + \underbrace{\langle v, b \rangle + \delta_{\mathcal{D}}(v) + \sigma_{\mathcal{C}}(z - s)}_{=: h_{D,2}(v, z)}. \quad (153)$$

As both parts of the objectives are proper, convex and lsc, it suffices to show additivity of the subdifferentials [RW04, Cor. 10.9] [Eck89, Thm. 3.15] [Eck89, Prop. 3.20, Prop. 3.19] [EB92]. Due to the boundedness of  $\mathcal{C}$  and  $\mathcal{D}$ ,

$$\begin{aligned} \text{ri}(\text{dom } h_2) \cap \text{ri}(\text{dom } h_1) &= (\text{ri}(\mathcal{C}) \times \mathbb{R}^{ndl}) \cap \{Lu = w\} \\ &= \{(u, Lu) | u \in \text{ri}(\mathcal{C})\}, \end{aligned} \quad (154)$$

$$\begin{aligned} \text{ri}(\text{dom } h_{D,2}) \cap \text{ri}(\text{dom } h_{D,1}) &= (\text{ri}(\mathcal{D}) \times \mathbb{R}^{nl}) \cap \{-L^\top v = z\} \\ &= \{(v, -L^\top v) | v \in \text{ri}(\mathcal{D})\}. \end{aligned} \quad (155)$$

Both of these sets are nonempty as  $\text{ri}(\mathcal{C}) \neq \emptyset \neq \text{ri}(\mathcal{D})$ . This implies additivity of the subdifferentials for the proposed objective [RW04, Cor. 10.9] and thus convergence (in the iterates as well as the objective) of the tight Douglas-Rachford iteration (cf. [Eck89, Thm. 3.15]).

We will now show that the primal and dual algorithms essentially generate the same iterates, i.e. from  $\tau := \tau_P = 1/\tau_D$ ,  $\bar{u}^{(k)} = \tau \bar{z}^{(k)}$  and  $\bar{w}^{(k)} = \tau \bar{v}^{(k)}$ , it follows that  $\bar{u}^{(k+1)} = \tau \bar{z}^{(k+1)}$ ,  $\bar{w}^{(k+1)} = \tau \bar{v}^{(k+1)}$  and  $u^{(k)} = z''^{(k)}$ ,  $v^{(k)} = w''^{(k)}$ . The last two equalities follow immediately from the previous ones by definition of the algorithms. Furthermore,

$$\begin{aligned} \bar{v}^{(k+1)} &= \bar{v}^{(k)} + v'^{(k)} - v^{(k)} \\ &= \bar{v}^{(k)} + (I + LL^\top)^{-1} \\ &\quad \cdot ((2v^{(k)} - \bar{v}^{(k)}) + (-L)(\bar{z}^{(k)} - 2\tau^{-1}z''^{(k)})) - v^{(k)} \end{aligned} \quad (156)$$

$$\begin{aligned} &= \tau^{-1}\bar{w}^{(k)} + (I + LL^\top)^{-1}((2w''^{(k)} - \tau^{-1}\bar{w}^{(k)}) \\ &\quad + (-L)(\tau^{-1}\bar{u}^{(k)} - 2\tau^{-1}u^{(k)})) - w''^{(k)} \end{aligned} \quad (157)$$

$$\begin{aligned} &= \tau^{-1}\bar{w}^{(k)} + (I + LL^\top)^{-1}(2w''^{(k)} - \tau^{-1}\bar{w}^{(k)}) - w''^{(k)} \\ &\quad - (I + LL^\top)^{-1}L(\tau^{-1}\bar{u}^{(k)} - 2\tau^{-1}u^{(k)}). \end{aligned} \quad (158)$$

By the Woodbury identity,  $(I + LL^\top)^{-1} = I - L(I + L^\top L)^{-1}L^\top$  and in particular  $(I + LL^\top)^{-1}L = L(I + L^\top L)^{-1}$ , therefore

$$\begin{aligned} \bar{v}^{(k+1)} &= \tau^{-1}\bar{w}^{(k)} + 2w''^{(k)} - \tau^{-1}\bar{w}^{(k)} \\ &\quad - L(I + L^\top L)^{-1}L^\top(2w''^{(k)} - \tau^{-1}\bar{w}^{(k)}) - w''^{(k)} \\ &\quad - L(I + L^\top L)^{-1}(\tau^{-1}\bar{u}^{(k)} - 2\tau^{-1}u^{(k)}) \end{aligned} \quad (159)$$

$$\begin{aligned} &= w''^{(k)} - L(I + L^\top L)^{-1} \\ &\quad \cdot (L^\top(2w''^{(k)} - \tau^{-1}\bar{w}^{(k)}) + (\tau^{-1}\bar{u}^{(k)} - 2\tau^{-1}u^{(k)})) \end{aligned} \quad (160)$$

$$\begin{aligned} &= \tau^{-1}L(I + L^\top L)^{-1} \\ &\quad \cdot ((2u^{(k)} - \bar{u}^{(k)}) + L^\top(\bar{w}^{(k)} - 2\tau w''^{(k)})) + w''^{(k)} \end{aligned} \quad (161)$$

$$= \tau^{-1}(Lu'^{(k)} + \tau w''^{(k)}) = \tau^{-1}\bar{w}^{(k+1)}. \quad (162)$$

By primal-dual symmetry, the same proof shows that  $\bar{u}^{(k+1)} = \tau \bar{z}^{(k+1)}$ . To conclude, we have shown that  $w''^{(k)} = v^{(k)}$  for  $\tau_D = 1/\tau$  and suitable initialization of the dual method. As the dual method was shown to converge,  $(w''^{(k)})$  must be a maximizing sequence for  $f_D$ . Together with the convergence of  $u^{(k)}$  to a minimizer of  $f$ , this proves the first part of the proposition. Equation (129) follows, as for any saddle-point  $(u^*, v^*)$ ,

$$f_D(w''^{(k)}) \leq f_D(v^*) = f(u^*) \leq f(u^{(k)}) \quad (163)$$

holds, and therefore  $f(u^{(k)}) - f(u^*) \geq 0$  and  $f(u^*) \geq f_D(w''^{(k)})$ .  $\square$

## References

- [AFP00] L. Ambrosio, N. Fusco, and D. Pallara. *Functions of Bounded Variation and Free Discontinuity Problems*. Clarendon Press, 2000.
- [AHU64] K. J. Arrow, L. Hurwicz, and H. Uzawa. *Studies in linear and non-linear programming. With contributions by Hollis B. Chenery [and others]*. Stanford University Press, 1964.

- [AT06] B. Appleton and H. Talbot. Globally minimal surfaces by continuous maximal flows. *Patt. Anal. Mach. Intell.*, 28:106–118, 2006.
- [Auj08] J.-F. Aujol. Some first-order algorithms for total variation based image restoration. *J. Math. Imaging Vis.*, 2008. published online.
- [BBC09] S. Becker, J. Bobin, and E. J. Candes. *NESTA: A Fast and Accurate First-order Method for Sparse Recovery*, April 2009.
- [BD86] J. P. Boyle and R. L. Dykstra. A method for finding projections onto the intersections of convex sets in Hilbert spaces. *Lecture Notes in Statistics*, 37:28–47, 1986.
- [Ber09] B. Berkels. An unconstrained multiphase thresholding approach for image segmentation. In *Scale Space and Var. Meth.*, volume 5567 of *Springer LNCS*, pages 26–37, 2009.
- [BG05] I. Borg and P. J. F. Groenen. *Modern Multidimensional Scaling*. Springer, 2nd edition, 2005.
- [BK04] Y. Boykov and V. Kolmogorov. An experimental comparison of min-cut/max-flow algorithms for energy minimization in vision. *Patt. Anal. Mach. Intell.*, 26(9):1124–1137, 2004.
- [Boy03] Y. Boykov. Computing geodesics and minimal surfaces via graph cuts. In *Int. Conf. Comp. Vis.*, pages 26–33, 2003.
- [Bra02] A. Braides. *Gamma-convergence for Beginners*. Oxford Univ. Press, 2002.
- [BT09] E. Bae and X.-C. Tai. Graph cut optimization for the piecewise constant level set method applied to multiphase image segmentation. In *Scale Space and Var. Meth.*, volume 5567 of *LNCS*, pages 1–13, 2009.
- [BVZ01] Y. Boykov, O. Veksler, and R. Zabih. Fast approximate energy minimization via graph cuts. *Patt. Anal. Mach. Intell.*, 23(11):1222–1239, 2001.
- [BYT10] E. Bae, J. Yuan, and X.-C. Tai. Global minimization for continuous multiphase partitioning problems using a dual approach. CAM Report 09-75, 2010.
- [CCP08] A. Chambolle, D. Cremers, and T. Pock. A convex approach for computing minimal partitions. Tech. Rep. 649, Ecole Polytechnique CMAP, 2008.
- [CD09] A. Chambolle and J. Darbon. On total variation minimization and surface evolution using parametric maximum flows. *Int. J. Comp. Vis.*, 84:288–307, 2009.
- [CEN06] T. F. Chan, S. Esedoğlu, and M. Nikolova. Algorithms for finding global minimizers of image segmentation and denoising models. *J. Appl. Math.*, 66(5):1632–1648, 2006.

- [CP08] P. L. Combettes and J.-C. Pesquet. A proximal decomposition method for solving convex variational inverse problems. *Inverse Problems*, 24(6), 2008.
- [CP10] A. Chambolle and T. Pock. A first-order primal-dual algorithm for convex problems with applications to imaging. *J. Math. Imaging Vision*, 2010. published online.
- [DAV08] V. Duval, J.-F. Aujol, and L. Vese. A projected gradient algorithm for color image decomposition. *CMLA Preprint*, (2008-21), 2008.
- [DFPH09] A. Delaunoy, K. Fundana, E. Prados, and A. Heyden. Convex multi-region segmentation on manifolds. In *Int. Conf. Comp. Vis.*, 2009.
- [DR56] J. Douglas and H. H. Rachford. On the numerical solution of heat conduction problems in two and three space variables. *Trans. of the AMS*, 82(2):421–439, 1956.
- [EB92] J. Eckstein and D. P. Bertsekas. On the Douglas-Rachford splitting method and the proximal point algorithm for maximal monotone operators. *Math. Prog.*, 55:293–318, 1992.
- [Eck89] J. Eckstein. *Splitting Methods for Monotone Operators with Application to Parallel Optimization*. PhD thesis, MIT, 1989.
- [FR60] W. H. Fleming and R. Rishel. An integral formula for total gradient variation. *Archiv der Mathematik*, 11(1):218–222, 1960.
- [GBO09] T. Goldstein, X. Bresson, and S. Osher. Geometric applications of the split bregman method: Segmentation and surface reconstruction. CAM Report 09-06, UCLA, 2009.
- [GM89] N. Gaffke and R. Mathar. A cyclic projection algorithm via duality. *Metrika*, 36(1):29–54, 1989.
- [GM09] D. Goldfarb and S. Ma. Fast multiple splitting algorithms for convex optimization. arXiv Preprint 0912.4570, 2009.
- [Gol64] A. A. Goldstein. Convex programming in hilbert space. *Bull. Amer. Math. Soc.*, 70:709–710, 1964.
- [Gow85] J.C. Gower. Properties of Euclidean and non-Euclidean distance matrices. *Lin. Alg. and its Appl.*, 67:81–97, 1985.
- [Gra81] A. Graham. *Kronecker Products and Matrix Calculus with Applications*. J. Wiley and Sons, NY, 1981.
- [Ish03] H. Ishikawa. Exact optimization for Markov random fields with convex priors. *Patt. Anal. Mach. Intell.*, 25(10):1333–1336, 2003.
- [JT95] C. R. Johnson and P. Tarazaga. Connections between the real positive semidefinite and distance matrix completion problems. *Lin. Alg. and its Appl.*, 223–224:375–391, 1995.



- [KB05] V. Kolmogorov and Y. Boykov. What metrics can be approximated by geo-cuts, or global optimization of length/area and flux. *Int. Conf. Comp. Vis.*, 1:564–571, 2005.
- [KT99] J.M. Kleinberg and E. Tardos. Approximation algorithms for classification problems with pairwise relationships: Metric labeling and Markov random fields. In *Found. Comp. Sci.*, pages 14–23, 1999.
- [KT07] N. Komodakis and G. Tziritas. Approximate labeling via graph cuts based on linear programming. *Patt. Anal. Mach. Intell.*, 29(8):1436–1453, 2007.
- [LBS09] J. Lellmann, F. Becker, and C. Schnörr. Convex optimization for multi-class image labeling with a novel family of total variation based regularizers. In *Int. Conf. Comp. Vis.*, 2009.
- [LBS10] J. Lellmann, D. Breitenreicher, and C. Schnörr. Fast and exact primal-dual iterations for variational problems in computer vision. In *Europ. Conf. Comp. Vis.*, volume 6312 of *LNCS*, pages 494–505, 2010.
- [LKY<sup>+</sup>09] J. Lellmann, J. Kappes, J. Yuan, F. Becker, and C. Schnörr. Convex multi-class image labeling by simplex-constrained total variation. In *Scale Space and Var. Meth.*, volume 5567 of *LNCS*, pages 150–162, 2009.
- [LLT06] J. Lie, M. Lysaker, and X.-C. Tai. A variant of the level set method and applications to image segmentation. *Math. Comp.*, 75:1155–1174, 2006.
- [LM79] P. L. Lions and B. Mercier. Splitting algorithms for the sum of two nonlinear operators. *SIAM J. Num. Anal.*, 16(6):964–979, 1979.
- [LP66] E.S. Levitin and B.T. Polyak. Constrained minimization problems. *U.S.S.R. Comput. Math. Math. Phys.*, 6:1–50, 1966.
- [Mic86] C. Michelot. A finite algorithm for finding the projection of a point onto the canonical simplex of  $\mathbb{R}^n$ . *J. Optim. Theory and Appl.*, 50(1):195–200, 1986.
- [MS89] D. Mumford and J. Shah. Optimal approximations by piecewise smooth functions and associated variational problems. *Comm. Pure Appl. Math.*, 42:577–685, 1989.
- [Mur03] K. Murota. *Discrete Convex Analysis*. SIAM, 2003.
- [Nes04] Y. Nesterov. Smooth minimization of non-smooth functions. *Math. Prog.*, 103(1):127–152, 2004.
- [Ols09] C. Olsson. *Global Optimization in Computer Vision: Convexity, Cuts and Approximation Algorithms*. PhD thesis, Lund University, 2009.

- [PCBC09a] T. Pock, D. Cremers, H. Bischof, and A. Chambolle. An algorithm for minimizing the Mumford-Shah functional. In *Int. Conf. Comp. Vis.*, 2009.
- [PCBC09b] T. Pock, D. Cremers, H. Bischof, and A. Chambolle. Global solutions of variational models with convex regularization. Technical report, Graz Univ. of Tech., 2009. Preprint.
- [PCF06] N. Paragios, Y. Chen, and O. Faugeras, editors. *The Handbook of Mathematical Models in Computer Vision*. Springer, 2006.
- [Pop80] L. D. Popov. A modification of the Arrow-Hurwicz method for search of saddle points. *Math. Notes*, 28:845–848, 1980.
- [Roc70] R.T. Rockafellar. *Convex Analysis*. Princeton UP, 1970.
- [ROF92] L. Rudin, S. Osher, and E. Fatemi. Nonlinear total variation based noise removal algorithms. *Physica D*, 60:259–268, 1992.
- [RW04] R.T. Rockafellar and R. J.-B. Wets. *Variational Analysis*. Springer, 2nd edition, 2004.
- [Set09a] S. Setzer. Split Bregman algorithm, Douglas-Rachford splitting and frame shrinkage. In *Scale Space and Variational Methods in Computer Vision*, volume 5567 of *LCNS*, pages 464–476, 2009.
- [Set09b] S. Setzer. *Splitting Methods in Image Processing*. PhD thesis, University of Mannheim, September 2009.
- [SR96] G. Sapiro and D. L. Ringach. Anisotropic diffusion of multi-valued images with applications to color filtering. In *Trans. Image Process.*, volume 5, pages 1582–1586, 1996.
- [Str83] G. Strang. Maximal flow through a domain. *Math. Prog.*, 26:123–143, 1983.
- [Str99] G. Strang. The discrete cosine transform. *SIAM Review*, 41(1):135–147, 1999.
- [SZS<sup>+</sup>06] R. Szeliski, R. Zabih, D. Scharstein, O. Veksler, V. Kolmogorov, A. Agarwala, M. Tappen, and C. Rother. A comparative study of energy minimization methods for Markov random fields. In *Europ. Conf. Comp. Vis.*, volume 2, pages 19–26, 2006.
- [TPCB08] W. Trobin, T. Pock, D. Cremers, and H. Bischof. Continuous energy minimization by repeated binary fusion. In *ECCV*, volume 4, pages 667–690, 2008.
- [WABF07] P. Weiss, G. Aubert, and L. Blanc-Féraud. Efficient schemes for total variation minimization under constraints in image processing. Tech. Rep. 6260, INRIA, 2007.
- [Win06] G. Winkler. *Image Analysis, Random Fields and Markov Chain Monte Carlo Methods*. Springer, 2006.

- [WSV00] H. Wolkowicz, R. Saigal, and L. Vandenberghe, editors. *Handbook of Semidefinite Programming*. Kluwer Academic Publishers, 2000.
- [WX04] C. Wang and N. Xiu. Convergence of the gradient projection method for generalized convex minimization. *Comp. Opt. Appl.*, 16:111–120, 2004.
- [Xu00] S. Xu. Estimation of the convergence rate of Dykstra’s cyclic projections algorithm in polyhedral case. *Acta Mathematicae Applicatae Sinica*, 16(2):217–220, 2000.
- [ZC08] M. Zhu and T. Chan. An efficient primal-dual hybrid gradient algorithm for total variation image restoration. CAM Report 08-34, UCLA, 2008.
- [ZGFN08] C. Zach, D. Gallup, J.-M. Frahm, and M. Niethammer. Fast global labeling for real-time stereo using multiple plane sweeps. In *Vis. Mod. Vis*, 2008.
- [Zie89] W.P. Ziemer. *Weakly Differentiable Functions*. Springer, 1989.
- [ZNF09] C. Zach, M. Niethammer, and J.-M. Frahm. Continuous maximal flows and Wulff shapes: Application to MRFs. In *Comp. Vis. Patt. Recogn.*, pages 1911–1918, 2009.